remote sensing

MDPI

Article

Diurnal Cycle in Surface Incident Solar Radiation Characterized by CERES Satellite Retrieval

Lu Lu and Qian Ma *

State Key Laboratory of Earth Surface Processes and Resource Ecology, College of Global Change and Earth System Science, Faculty of Geographical Science, Beijing Normal University, Beijing 100875, China; 202121490006@mail.bnu.edu.cn

* Correspondence: maqian@bnu.edu.cn

Abstract: Surface incident solar radiation (R_s) plays an important role in climate change on Earth. Recently, the use of satellite-retrieved datasets to obtain global-scale R_s with high spatial and temporal resolutions has become an indispensable tool for research in related fields. Many studies were carried out for R_s evaluation based on the monthly satellite retrievals; however, few evaluations have been performed on their diurnal variation in R_s. This study used independently widely distributed ground-based data from the Baseline Surface Radiation Network (BSRN) to evaluate hourly R_s from the Clouds and the Earth's Radiant Energy System Synoptic (CERES) SYN1deg–1Hour product through a detrended standardization process. Furthermore, we explored the influence of cloud cover and aerosols on the diurnal variation in R_s. We found that CERES-retrieved R_s performs better at midday than at 7:00–9:00 and 15:00–17:00. For spatial distribution, CERES-retrieved R_s performs better over the continent than over the island/coast and polar regions. The Bias, MAB and RMSE in CERES-retrieved R_s under clear-sky conditions are rather small, although the correlation coefficients are slightly lower than those under overcast-sky conditions from 9:00 to 15:00. In addition, the range in R_s bias caused by cloud cover is 1.97–5.38%, which is significantly larger than 0.31–2.52% by AOD.

Keywords: BSRN; CERES; solar radiation; diurnal variation

Citation: Lu, L.; Ma, Q. Diurnal Cycle in Surface Incident Solar Radiation Characterized by CERES Satellite Retrieval. *Remote Sens.* **2023**, *15*, 3217. https://doi.org/10.3390/rs15133217

Academic Editors: Jesús Polo and Dmitry Efremenko

Received: 11 May 2023
Revised: 14 June 2023
Accepted: 15 June 2023
Published: 21 June 2023

1. Introduction

Surface incident solar radiation (R_s) plays an important role in climate change as it is the major energy source in the Earth system [1,2]. The performance of R_s is closely related to water cycle, as it significantly affects the evaporation of surface water [3]. Robock et al. [4] have shown that the changes in soil temperature are consistent with those in R_s during the global brightening and dimming period. Changes in R_s affect the melting and growth of glaciers as well [5]; for example, the snow cover in the northern hemisphere did not change significantly before the 1980s but exhibited a sharp downward trend in the brightening period after the 1980s [6]. Several studies suggest that R_s also has an impact on ecosystems, driving crop growth as an energy factor [7,8]. In addition, the spatial and temporal distribution of R_s is the basis for energy policy decision making on solar power [9]. Therefore, decreases and increases in R_s (also known as global dimming and brightening, respectively) have received widespread attention [10–12]. The variations in cloud cover, aerosols, and other factors were also explored, as they contributed more to the change in R_s [13,14]. Cloud cover regulates the radiative energy balance of the atmosphere [15]. Compared with a clear-sky atmosphere, cloud cover can absorb and reflect a large amount of incident shortwave radiation, which has a cooling effect on the subsurface. Aerosols can absorb and scatter solar radiation, which can block incident solar radiation, especially by reducing the passage of ultraviolet rays, weakening the solar radiation reaching the ground [16].

The diurnal cycle in R_s due to the Earth's rotation can cause diurnal changes in the surface and atmospheric state in all regions except the polar regions (where solar variability is more seasonal) through a variety of physical processes [17]. Ye et al. [18] noted that the diurnal temperature range (DTR) decreased rapidly in China from the 1960s to the 1980s when it became significantly dimmer, while in the early 1990s, the decline in DTR stopped during the period when R_s changed from dimming to brightening, which was confirmed by Du et al. [19]. Both sea surface temperature variability in the western Pacific warm pool [20] and the diurnal behavior of the spiral rainbands [21] are modulated by the diurnal cycle in R_s.

Currently, R_s can be obtained from ground-based observations, reanalyses datasets, and satellite-retrieved datasets [22–24]. The ground-based observations of R_s have the highest accuracy but are sparsely distributed [9]. Reanalyses datasets have better spatial continuity, but the bias in cloud and aerosol simulations can lead to low accuracy in R_s [25,26]. The accuracy of the satellite retrieved data is relatively higher than that of reanalyses, as clouds and aerosols observed by satellite were used in the radiative transfer model [27].

Most studies have evaluated satellite-retrieved R_s on monthly and annual time scales. These studies have shown that satellite-retrieved datasets are less biased and have better accuracy than reanalyses datasets at long time scales [14,28,29]. However, few evaluations have been performed on satellite-retrieved R_s on the diurnal scale. Therefore, a comprehensive and detailed evaluation of satellite-retrieved R_s on an hourly scale is needed. In this study, we compared Clouds and the Earth's Radiant Energy System Synoptic (CERES)-retrieved hourly R_s with Baseline Solar Radiation Network (BSRN) observations to quantify their differences in the diurnal cycle of R_s. Furthermore, the influence of clouds and aerosols on the diurnal variation in R_s was explored.

2. Data and Methods

2.1. Ground-Based Observation Data

Ground-based observation data with high-quality instrumentation and long-term maintenance provide the most reliable and accurate R_s [9]. In 1988, the WMO proposed the establishment of a new international ground-based radiation baseline network (i.e., BSRN) under the World Climate Research Program (WCRP) [30]. BSRN provides high-temporal resolution ground-based radiation observations (1 min) that can be used to validate satellite-retrieved datasets, improve radiative transfer calculations in climate models, and support the detection and monitoring of long-term changes in ground-based radiation fluxes [31].

In this study, we use ground-based observations from the BSRN to evaluate the satellite-retrieved dataset. As CERES data began in March 2000, the research period in this study is March 2000–July 2021. Seventy–three stations observed R_s during this period, as shown in Figure 1. Figure 2 shows the length of the record at each site. Twenty sites marked in red were excluded because their recorded periods were less than 4 years. Finally, 53 sites marked in blue color were used for evaluation in this work. Of these, 38 are located on the continent, 8 are located on the continent along the island/coast, and 8 are located on the continent in the polar region.

Thermophile radiometers suffer a negative bias because of the infrared loss to the sky at nighttime [32]. Consequently, measurement data at nighttime were abandoned in this study. We focus on the period from 7:00 to 17:00 each day, as the sample size of the data in this period is larger than 200,000 (see Figure 3), accounting for more than 50% of the data for each hour.

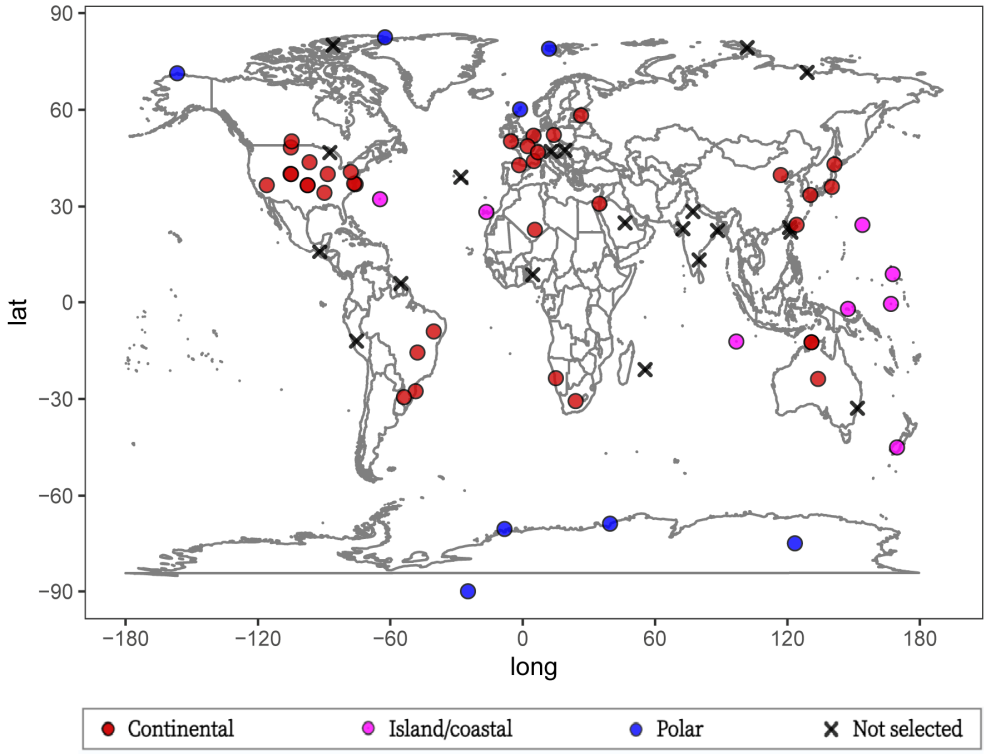

Figure 1. Geographical distribution of observation sites used for the evaluation of satellite-retrieved R_s data. The blue, red, and magenta circles indicate the site location in the polar (Arctic or Antarctic), continent, and island/coast, respectively. The black crosses indicate the sites excluded in this study as fewer data were available.

2.2. Satellite-Retrieved Dataset

Clouds and the Earth's Radiant Energy System (CERES) is an investigation to provide earth radiation budget data through satellite sensing, which is produced, archived, and made available to the scientific community by the Atmospheric Sciences Data Center (ASDC), the Langley Research Center (LaRC), and the National Aeronautics and Space Administration (NASA) [33].

The CERES SYN Ed4.1 product contains hourly R_s, cloud cover, and aerosol optical depths with a $1^\circ \times 1^\circ$ spatial resolution. Cloud properties from high-resolution imagers on several satellites were precisely matched with broadband radiance data. CERES has been providing clouds since 2000 using the algorithm developed for the second edition of CERES (Ed2) until 2002. To improve the accuracy of the clouds, CERES Edition 4 (Ed4) applies the revised algorithm [34]. The aerosols are from the Multi-scale Atmospheric Transport and Chemistry (MATCH) model constituents and the NASA-GSFC Moderate-resolution Imaging Spectroradiometer (MODIS) MOD04_L2/MYD04_L2 products [35]. The clouds and aerosols are used as inputs of the Fu–Liou radiative transfer model. Additional inputs are pressure, temperature and water vapor profiles from the Global Modeling and Assimilation Office (GMAO) Goddard Earth Observing System Model (GEOS). Gaseous absorption in the shortwave region is treated by the method described in Kato et al. [36], and absorption by water vapor, carbon dioxide, ozone, methane and oxygen were considered. Then, the adjusted fluxes were derived by constraining the calculated at the top of the atmosphere (TOA) fluxes to the observed CERES TOA fluxes. R_s in the CERES-SYN Ed4.1 products were computed hourly in approximate equal-area grid boxes [37].

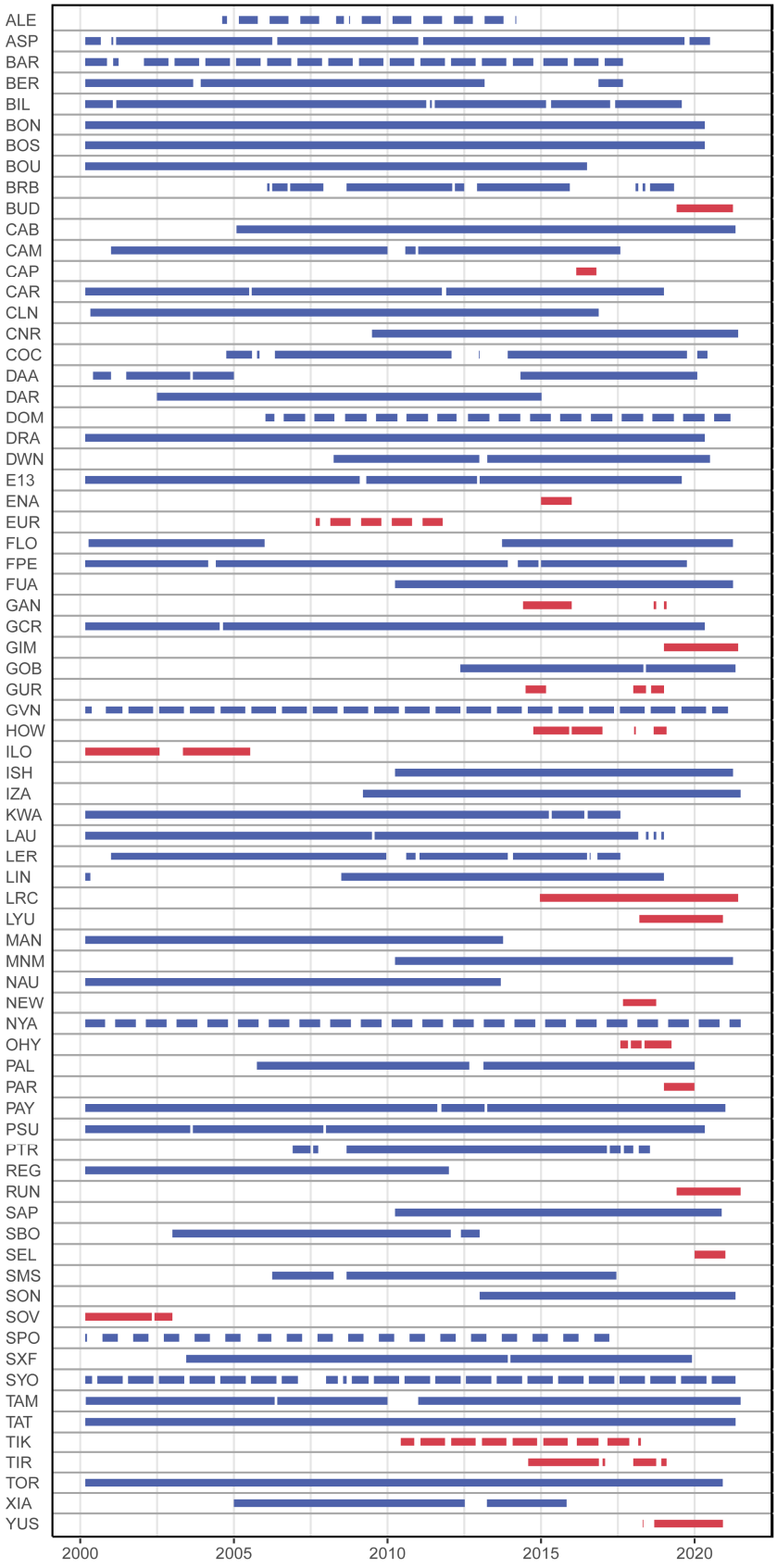

Figure 2. Time duration of each site in BSRN for 2000–2021. Red indicates that sites with short measurement periods are excluded from this work; blue indicates that sites are used in this work.

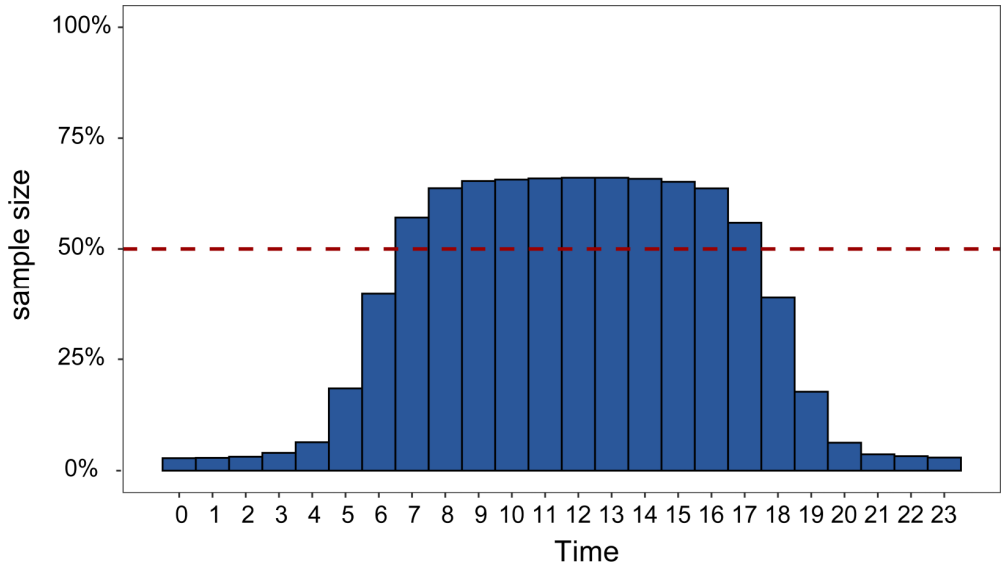

Figure 3. The sample size of the observation data at different times. The red line indicates 50% of the total sample size.

2.3. Methods

Taking into account that the R_s measurement stations are distributed throughout the Earth, we converted UTC to local time for subsequent evaluation. To reduce the diurnal cycle and seasonal cycle in the R_s on the evaluation results, the observational data and CERES retrieved data were standardized as follows:

$$SW_{i,std} = \frac{SW_i}{SW_{i,TOA}} \quad (1)$$

where $SW_{i,std}$ represents the standardized radiation value at hour i, SW_i represents the original radiation value at hour i and $SW_{i,TOA}$ represents the radiation value at the top of the atmosphere at hour i. Solar radiation at the top of atmosphere (SW_{TOA}) is affected by the solar zenith angle and Sun–Earth distance, so SW_{TOA} contains diurnal and seasonal variation, as shown in Figure 4. Both the observational R_s data and CERES retrieved R_s data were standardized by dividing SW_{TOA} from CERES. The standardized R_s data are greater than or equal to 0 and less than 1 and unitless. It is worth noting that the R_s appearing in the following is the standardized one.

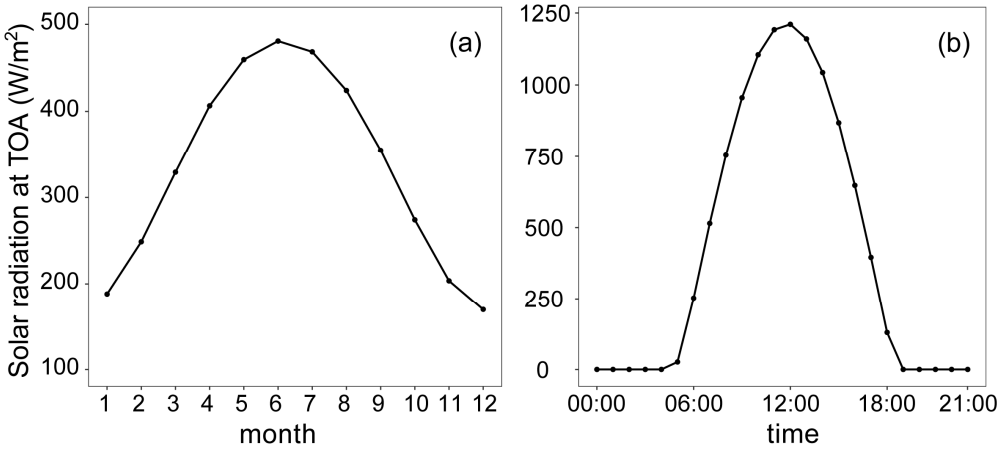

Figure 4. (**a**) Monthly solar radiation at TOA at XIA station in 2005; (**b**) hourly solar radiation at TOA at XIA station on 25 April 2005.

In this study, the Bias, mean absolute bias (MAB), root-mean-square error (RMSE), and correlation coefficient (R) are used to evaluate satellite radiation data with ground-based observations, as shown in Equations (2)–(5).

$$\text{Bias} = \frac{1}{n}\sum_{i=1}^{n}(S_i - O_i) \tag{2}$$

$$\text{MAB} = \frac{1}{n}\sum_{i=1}^{n}|S_i - O_i| \tag{3}$$

$$\text{RMSE} = \sqrt{\frac{\sum_{i=1}^{n}(S_i - O_i)^2}{n}} \tag{4}$$

$$\text{R} = \frac{\sum_{i=1}^{n}(S_i - \overline{S})(O_i - \overline{O})}{\sum_{i=1}^{n}(S_i - \overline{S})^2 \sum_{i=1}^{n}(O_i - \overline{O})^2} \tag{5}$$

where S_i is the satellite-retrieved R_s at hour i and O_i is the observed R_s at hour i. The mean absolute bias was used here to avoid the offsetting of positive and negative deviations.

3. Results

3.1. Difference between CERES-Retrieved and BSRN Hourly R_s

Most R_s data are in the range from 0.50 to 0.75, as shown in Figure 5l. Hourly R_s were underestimated by −1.10% in CERES. The MAB between satellite-retrieved and observed R_s is less than 10%, while the RMSE is 12.88% for the whole period. As the seasonal and diurnal cycles were removed, their correlation coefficient was 0.83, which is much less than 0.92 for calculation with absolute values. This is consistent with the value of 0.95 noted by David et al. [35].

Evaluations were also conducted each hour, as shown in Figure 5a–k. Hourly R_s retrieved by CERES show negative Bias from 7:00 to17:00, with the largest Bias of −2.29% at 7:00 and the smallest Bias of −0.43% at 13:00. The MAB ranges from 8.77% to 8.92% for 10:00–13:00 and is relatively large, 10.03% and 9.89%, for 7:00 and 17:00, respectively. For other hours, MAB ranges from 9.09% to 9.52%. It decreases until midday and increases afterward. The RMSE is smallest at 10:00 (12.51%) and largest at 7:00 (13.66%). The diurnal variation of RMSE is similar to that of MAB. R is higher than 0.8 most of the time, except at 7:00 and 17:00. R is higher at midday and lower at 7:00 and 17:00. These results suggest that the CERES-retrieved R_s performs better at midday than at 7:00–8:00 and 16:00–17:00. The smaller difference between satellite-retrieved and observed R_s from 10:00 to 13:00 may be attributed to the orbit overpass times related to the two sensors, Terra and Aqua. Terra is in a descending sun-synchronous orbit with an equator-crossing time at 10:30, while Aqua is in ascending sun-synchronous orbits with an equator-crossing time at 13:30 [38].

Most of the stations show negative Bias, especially at 7:00 and 17:00, and it is particularly evident for stations located along the island/coast (Figure 6 and Table A1). MAB and RMSE are especially larger at 7:00 and 17:00 with relatively smaller R for most stations, as shown in Figures 7–9 and Table A1. They perform better at midday. These are consistent with those shown in Figure 6. Notably, the largest Bias (−21.95% for Bias, 22.93% for MAB, 25.79% for RMSE, and 0.56 for R) was found at the IZA station located in Tenerife (Canary Islands, Spain) [39], which is consistent with the results of Hao et al. [40] and Tang et al. [22]. This may be attributed to its high altitude above the subtropical inversion layer, as cloud cover only affects the lower part of the area (below 2000 m), while the upper part of the island is cloudless [41].

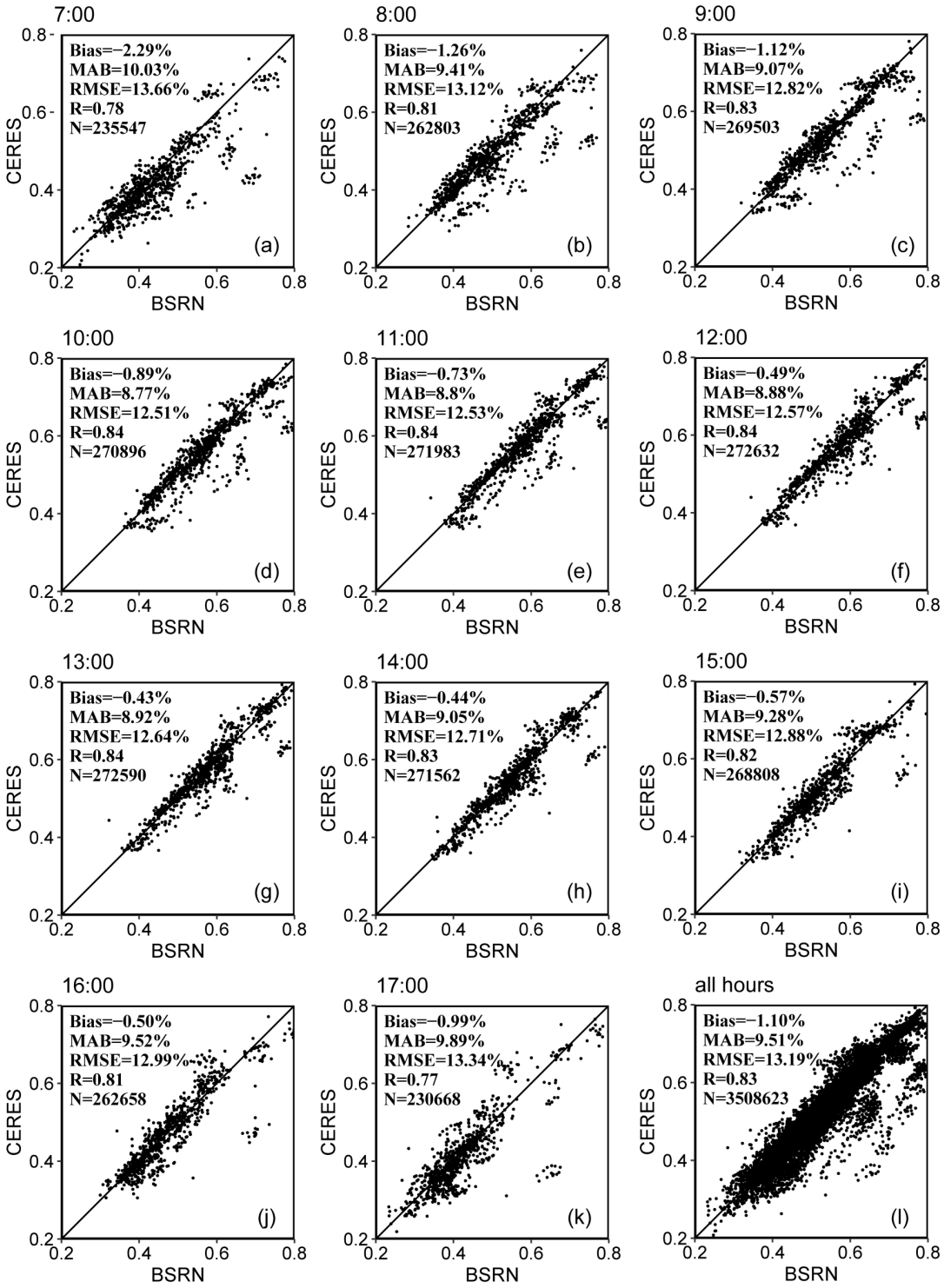

Figure 5. Scatter plots of annual average of hourly CERES retrieved and observed R_s from 2000 to 2021 for each hour from 7:00 to 17:00 and all hours. The statistical parameters in the upper left corner of (**a**–**l**) were calculated using R_s at 53 stations in Figure 1, and N is sample hours participating in the calculation.

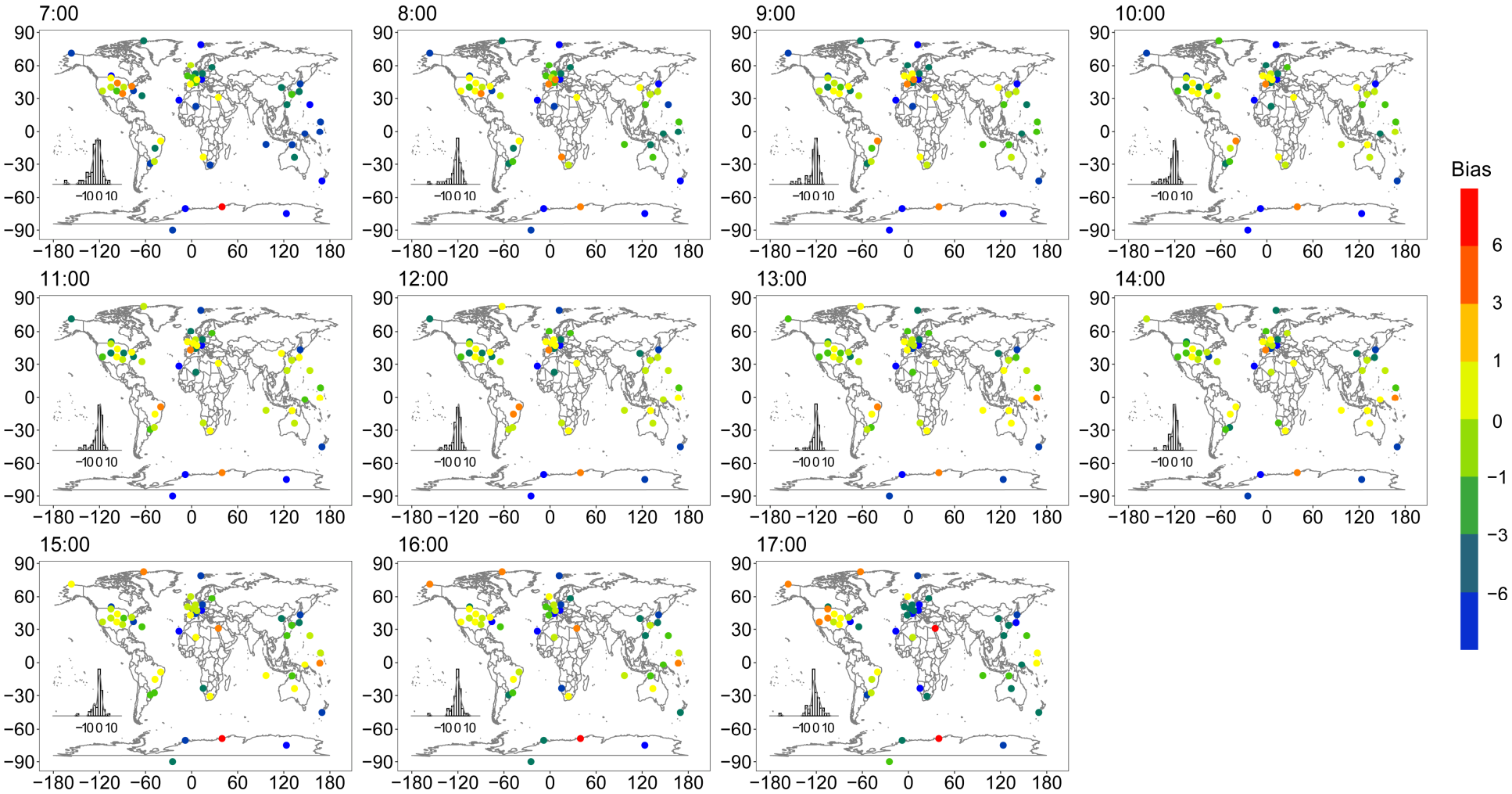

Figure 6. Bias between hourly CERES-retrieved R_s and observed R_s in each station for individual hours from 7:00 to 17:00. Unit: %.

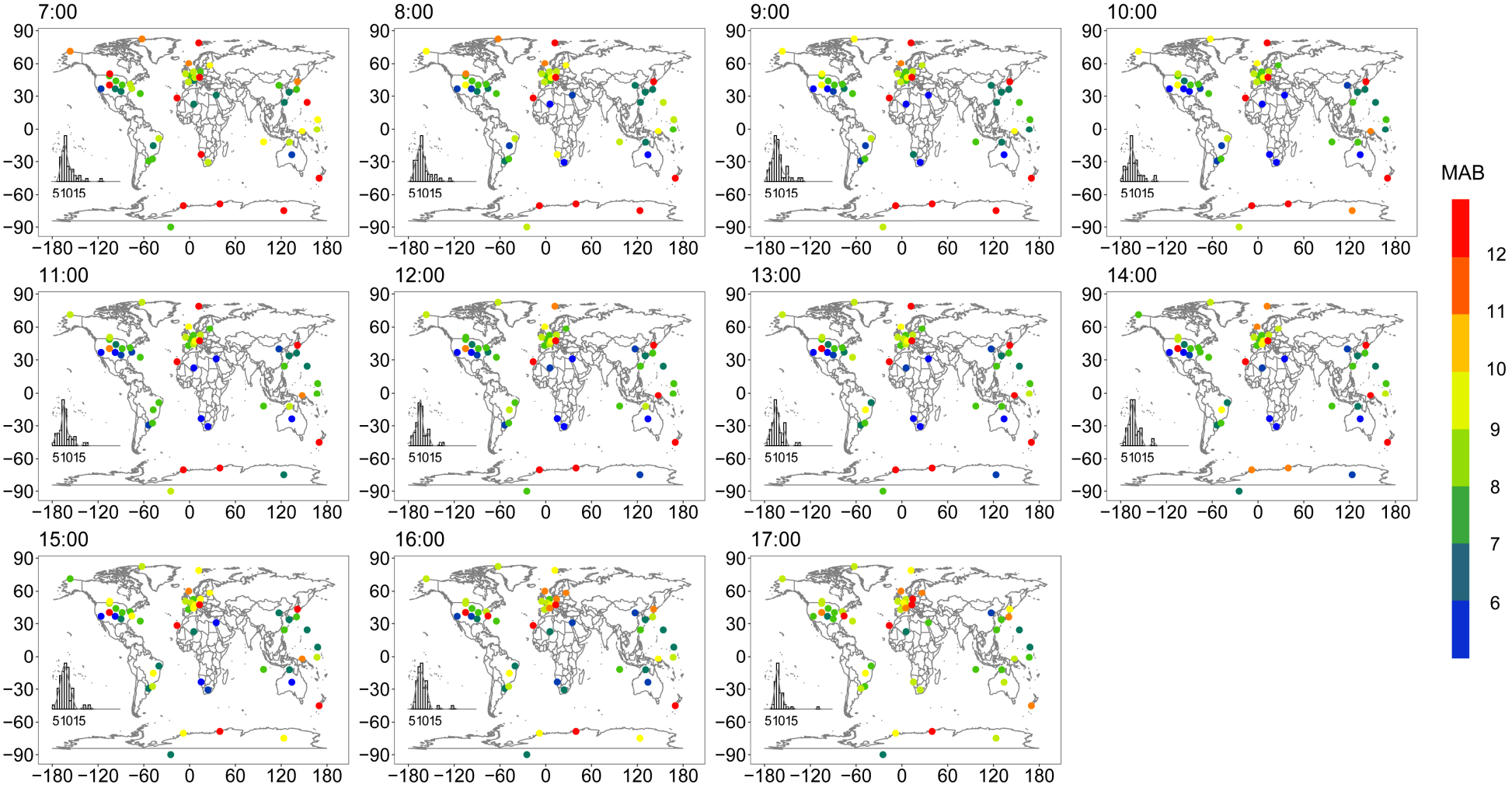

Figure 7. Mean absolute bias (MAB) between hourly CERES-retrieved R_s and observed R_s in each station for individual hours from 7:00 to 17:00. Unit: %.

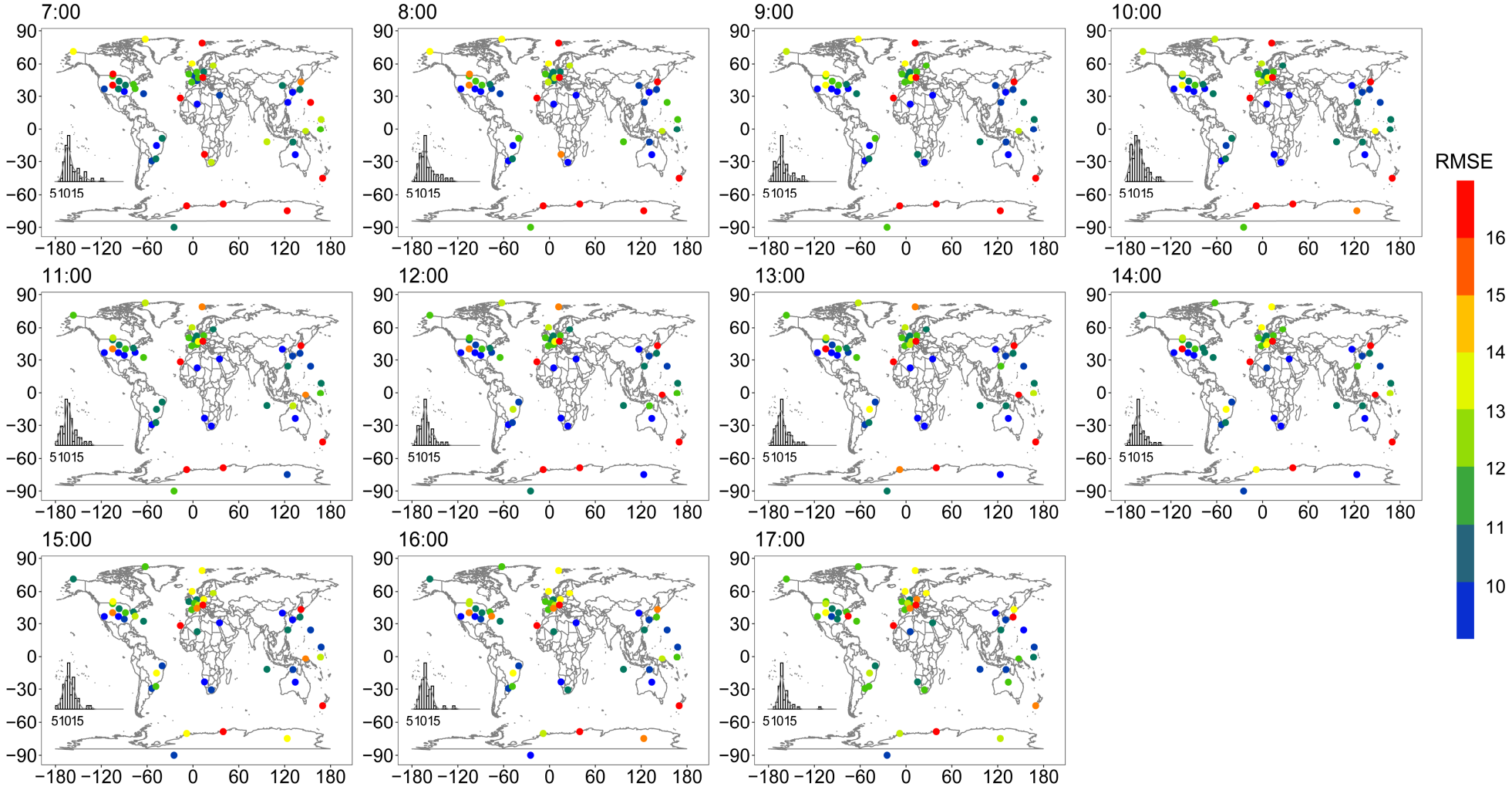

Figure 8. Root-mean-square error (RMSE) between hourly CERES-retrieved R_s and observed R_s in each station for individual hours from 7:00 to 17:00. Unit: %.

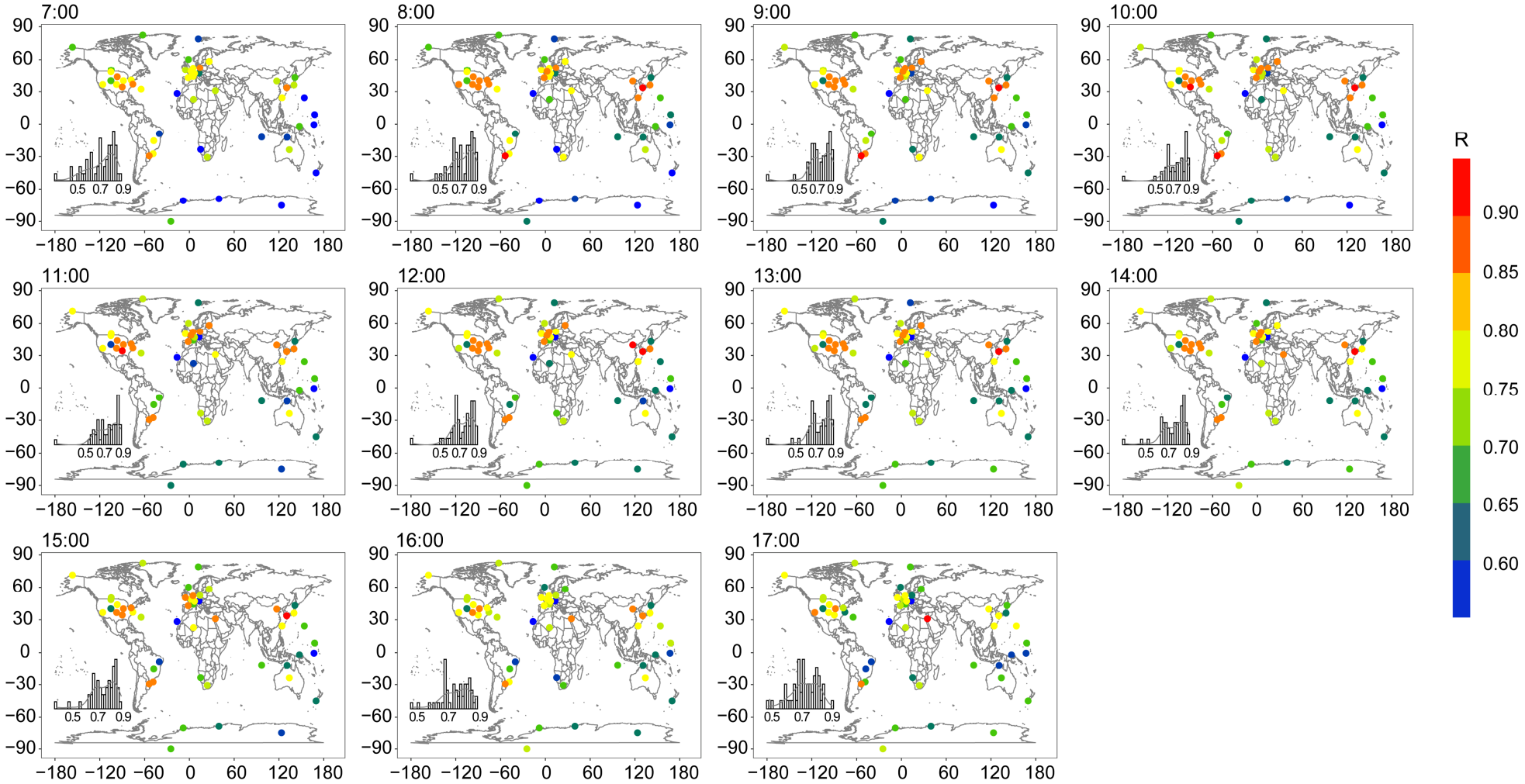

Figure 9. Correlation coefficients (R) between hourly CERES-retrieved R_s and observed R_s in each station for individual hours from 7:00 to 17:00.

Figure 10 and Table 1 summarize the statistical parameters for different types of stations. The negative Bias for the continental stations (−0.01–−1.38%) is smaller than that for the island/coastal stations (−1.84–−8.16%), and they are both underestimated more at 7:00 and 17:00 and less at midday. The stations located in the polar regions show the opposite variation, with negative Bias increasing until 9:00, then decreasing throughout the day and finally showing a positive Bias after 16:00. The MAB for continental stations ranges from 8.14% to 9.66%, which is smaller than that for island/coastal (10.67–13.54%) and polar (9.84–12.11%) stations. The RMSE for continental stations ranges from 11.44% to 12.51%, which again is smaller than that for island/coastal (13.94–16.93%) and polar (13.13–15.74%) stations. The R value for continental stations ranges from 0.74 to 0.80, which is higher than that for island/coastal (0.59–0.70) and polar (0.66–0.76) stations. The CERES-retrieved R_s performs better at most continental stations, although the spatial variabilities of these statistical parameters are relatively larger as they cover different land cover types, climate zones, and surface topography. Rapid weather changes and the presence of both land and water within the grid (edge effects) may lead to the worst performance along the island/coastal stations [40]. CERES-retrieved R_s data also perform relatively poorly at polar stations, which may be caused by the failure of cloud detection as more ice and snow exist in this region, and the temperature of clouds is usually not lower than that of surface snow and ice [31]. Additionally, Urraca et al. [41] pointed out the failure of most radiation products over polar regions, where strong intra-annual variations are present due to low solar elevation angles in winter, seasonal snowfall and the low viewing angle of satellites. The R_s difference over the continent is observed to be smaller than that along the island/coast and polar regions, which is confirmed by the findings in other studies [42,43].

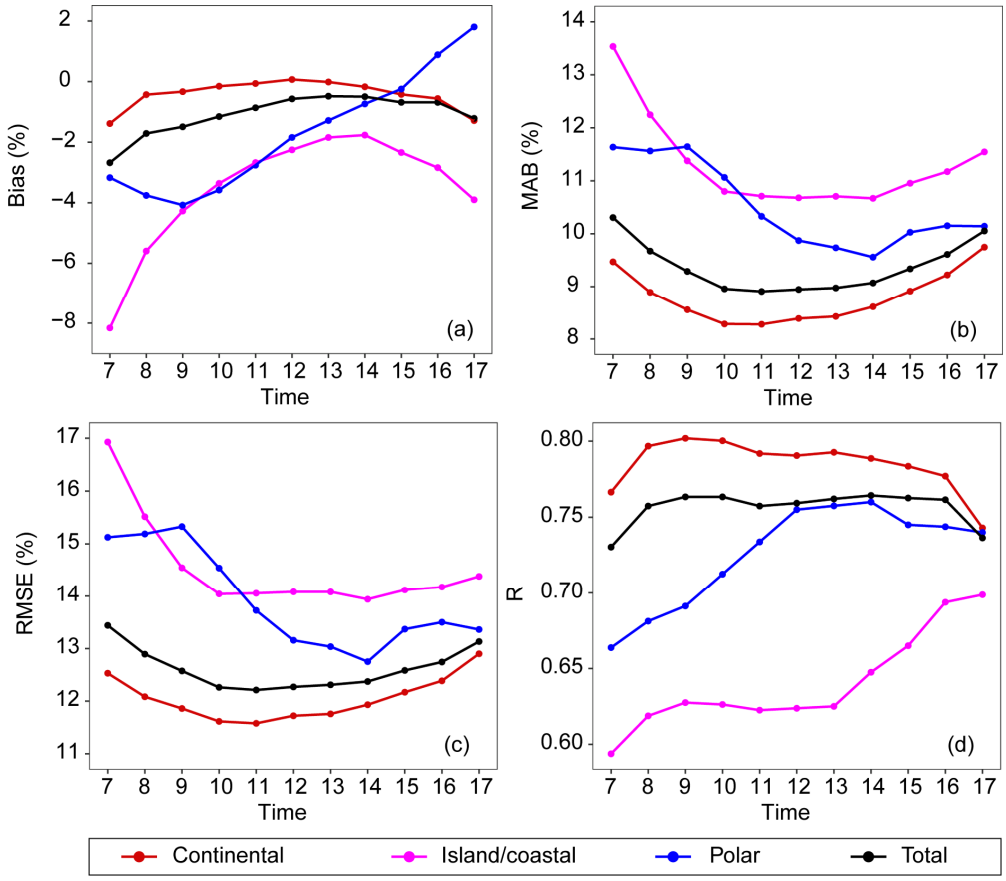

Figure 10. Diurnal variations of statistical parameters between hourly CERES-retrieved R_s and observed R_s for different types of sites. (**a**) Bias %; (**b**) Mean absolute bias (MAB) %; (**c**) Root-mean-square error (RMSE) %; and (**d**) Correlation coefficient (R).

Table 1. Evaluation of CERES hourly R_s against the ground-based measurements for different regions. Unit: Bias %, MAB %, RMSE %.

Region	Statistical Parameters	7:00	8:00	9:00	10:00	11:00	12:00	13:00	14:00	15:00	16:00	17:00
Continental	Bias	−1.38	−0.43	−0.33	−0.15	−0.06	0.07	−0.01	−0.17	−0.42	−0.56	−1.28
	MAB	9.30	8.72	8.36	8.14	8.24	8.38	8.43	8.59	8.80	9.11	9.66
	RMSE	12.36	12.05	11.82	11.52	11.44	11.56	11.60	11.74	11.86	11.97	12.51
	R	0.77	0.80	0.80	0.80	0.78	0.78	0.79	0.79	0.79	0.78	0.74
Island/coastal	Bias	−8.16	−5.59	−4.27	−3.36	−2.67	−2.25	−1.84	−1.76	−2.34	−2.84	−3.90
	MAB	13.54	12.25	11.38	10.80	10.71	10.68	10.71	10.67	10.96	11.17	11.55
	RMSE	16.93	15.51	14.54	14.04	14.06	14.08	14.08	13.94	14.12	14.18	14.38
	R	0.59	0.62	0.63	0.63	0.62	0.62	0.63	0.65	0.67	0.70	0.70
Polar	Bias	−3.17	−3.76	−4.07	−3.58	−2.76	−1.84	−1.28	−0.74	−0.25	0.89	1.81
	MAB	12.11	11.92	11.97	11.27	10.48	10.01	9.93	9.84	10.39	10.54	10.49
	RMSE	15.69	15.63	15.74	14.79	13.90	13.33	13.27	13.13	13.84	14.02	13.83
	R	0.66	0.68	0.69	0.72	0.74	0.76	0.76	0.76	0.74	0.74	0.74
Total	Bias	−2.68	−1.71	−1.49	−1.15	−0.86	−0.57	−0.48	−0.50	−0.68	−0.69	−1.21
	MAB	10.31	9.67	9.29	8.96	8.91	8.95	8.97	9.07	9.34	9.61	10.05
	RMSE	13.44	12.89	12.57	12.26	12.21	12.27	12.31	12.37	12.58	12.74	13.13
	R	0.73	0.76	0.76	0.76	0.76	0.76	0.76	0.76	0.76	0.76	0.74

3.2. Effect of Clouds and AOD on the Bias in CERES-Retrieved Hourly R_s

Cloud cover and aerosol optical depth (AOD) are two important factors that regulate R_s [13,44]. Some studies have shown that CERES-retrieved cloud cover is relatively accurate [34,45–47] and AOD has high accuracy with AERONET observations [48,49]. This section focuses on the CERES-retrieved R_s bias under different cloud cover and AOD (at 550 nm) categories.

Here, we define cloud cover of less than 20% as clear-sky, greater than 80% as overcast-sky and everything else as cloudy-sky. The Bias is smallest under clear-sky conditions as shown in Figure 11a, with the smallest value of approximately 0% at 9:00, slightly underestimated at midday (−0.16%) and overestimated at 14:00–17:00 (0.60%). Large underestimations in R_s were found under other two conditions especially for cloudy-sky conditions, with smaller negative Bias at midday (−1.36% for cloudy-sky, −0.09% for overcast-sky) and larger negative Bias at 7:00 and 17:00 (−3.84% for cloudy-sky, −1.92% for overcast-sky).

MAB and RMSE for all times under clear-sky conditions are significantly (3.33–7.01% for MAB and 5.84–10.31% for RMSE) smaller than those under cloudy-sky (9.96–11.91% for MAB and 13.42–15.20% for RMSE) and overcast-sky conditions (10.32–11.09% for MAB and 13.66–14.67% for RMSE), especially around midday (Figure 11b,c). Compared with cloudy-sky conditions, MAB and RMSE under overcast-sky conditions are 0.26–1.10% and 0.10–0.33% larger for 9:00–15:00. The diurnal cycle of MAB and RMSE is strongest (1.30% variation and 1.59% variation) under clear-sky conditions with low values (3.33% for MAB and 5.84% for RMSE) at midday and high values (7.01% for MAB and 10.31% for RMSE) at 7:00–9:00 and 15:00–17:00. They are rather stable for cloudy-sky (0.63% variation for MAB and 0.59% variation for RMSE) and overcast-sky (0.22% variation for MAB and 0.29% variation for RMSE) conditions.

Figure 11d shows that R under overcast-sky conditions (0.75–0.77) is higher than that under clear-sky conditions (0.69–0.74) for 9:00–15:00. CERES-retrieved R_s under cloudy-sky conditions has the lowest R for each hour, ranging from 0.49 at midday to ~0.60 at 7:00–9:00 and 16:00–17:00. MAB and RMSE under cloudy-sky conditions are similar to overcast-sky and all-sky conditions, but R is much lower. This may be attributed to the Bias under cloudy-sky conditions being 1.44% and 1.17% smaller than those under overcast-sky and all-sky conditions.

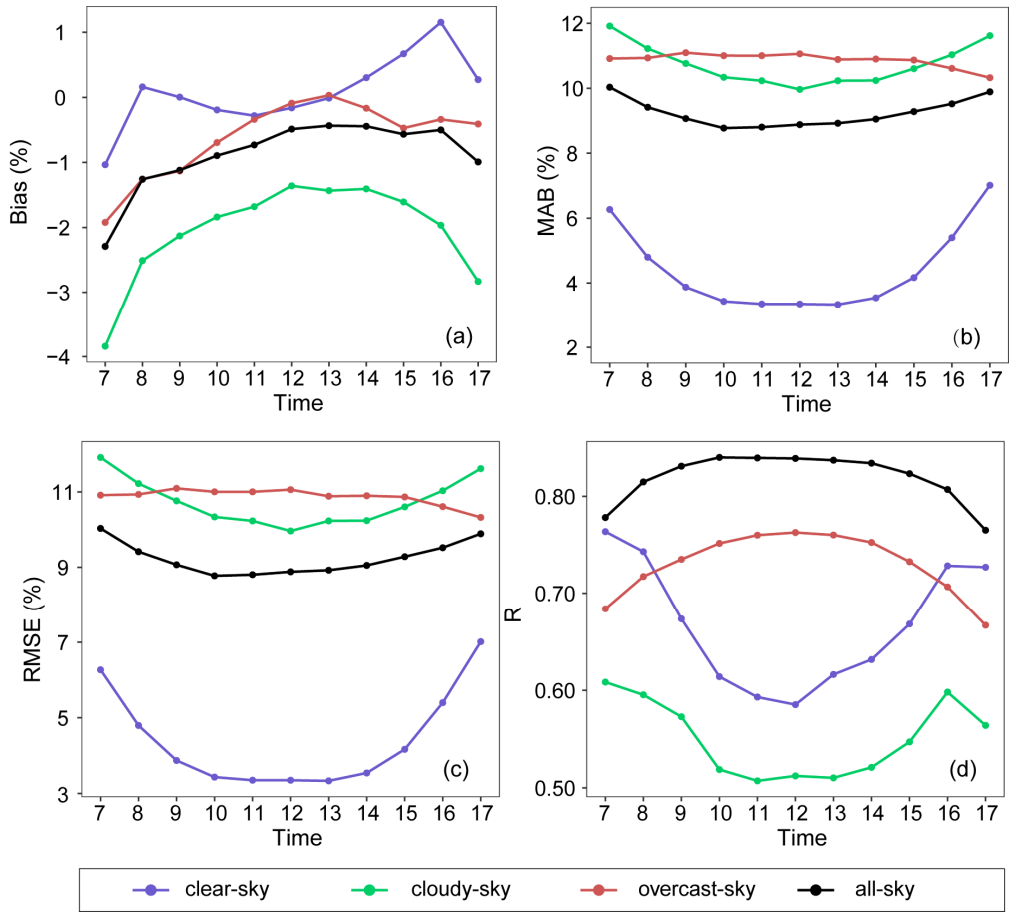

Figure 11. Diurnal variations of statistical parameters for CERES retrieved hourly R_s at all ground-based sites for different cloud cover conditions. (**a**) Bias %; (**b**) Mean absolute bias (MAB) %; (**c**) Root-mean-square error (RMSE) %; and (**d**) Correlation coefficient (R).

R is lower at midday and higher at 7:00 and 17:00 under clear-sky and cloudy-sky conditions, while it is the opposite under overcast-sky conditions. Under clear-sky and cloudy-sky conditions, MAB and RMSE decrease/increase while R also decreases/increases correspondingly, which is the opposite of the situation presented in Figure 10 (MAB and RMSE increase while R decreases and vice versa). This may be because more clouds are likely to appear at midday [50], and there are many broken clouds in low clouds. Broken clouds are smaller in size and more disperse in the sky, and their area may be much smaller than the single pixel of CERES satellite data. Thus, many broken clouds at these hours can easily be misjudged as clear-sky or cloudy-sky conditions. It is easier for the satellite to detect the circumstances under overcast-sky conditions. R is higher for all-sky conditions with more fluctuation than that for other conditions because R_s is more stable in the same cloud category.

Furthermore, we classified cloud cover more specifically into "0–20", "20–40", "40–60", "60–80", and "80–100" categories. The AOD values were divided into "0–0.05", "0.05–0.1", "0.1–0.15", "0.15–0.3" and "0.3–8" categories (see Figures 12 and 13). A negative Bias of R_s were found at almost all hours. Bias was the smallest, nearly zero, in the "0–20" and "80–100" cloud cover categories. This means that the R_s Bias is small under clear-sky conditions and cloudy-sky conditions. Bias, calculated by the mean method, is largest in the "60–80" cloud cover category for all hours, with the largest value of −4.71% at 7:00. Median values show that a larger negative Bias is shown in the "40–60" and "60–80" cloud cover categories, with the highest value of −5.38% at 7:00 for the "40–60" interval. At 17:00, the difference between the mean and the median values is the smallest. From

Table 2, we found changes in cloud cover contribute to 1.97–5.38% changes in R_s Bias, and the variation in R_s Biases caused by cloud cover is in the range of 0.86–2.43%. The change/variation in the median values (4.39–5.38%/1.98–2.43%) is larger than that in the mean values (1.97–4.03%/0.86–1.75%) as shown in Table 2, which may be due to the positive values being offset by the negative values for mean calculations.

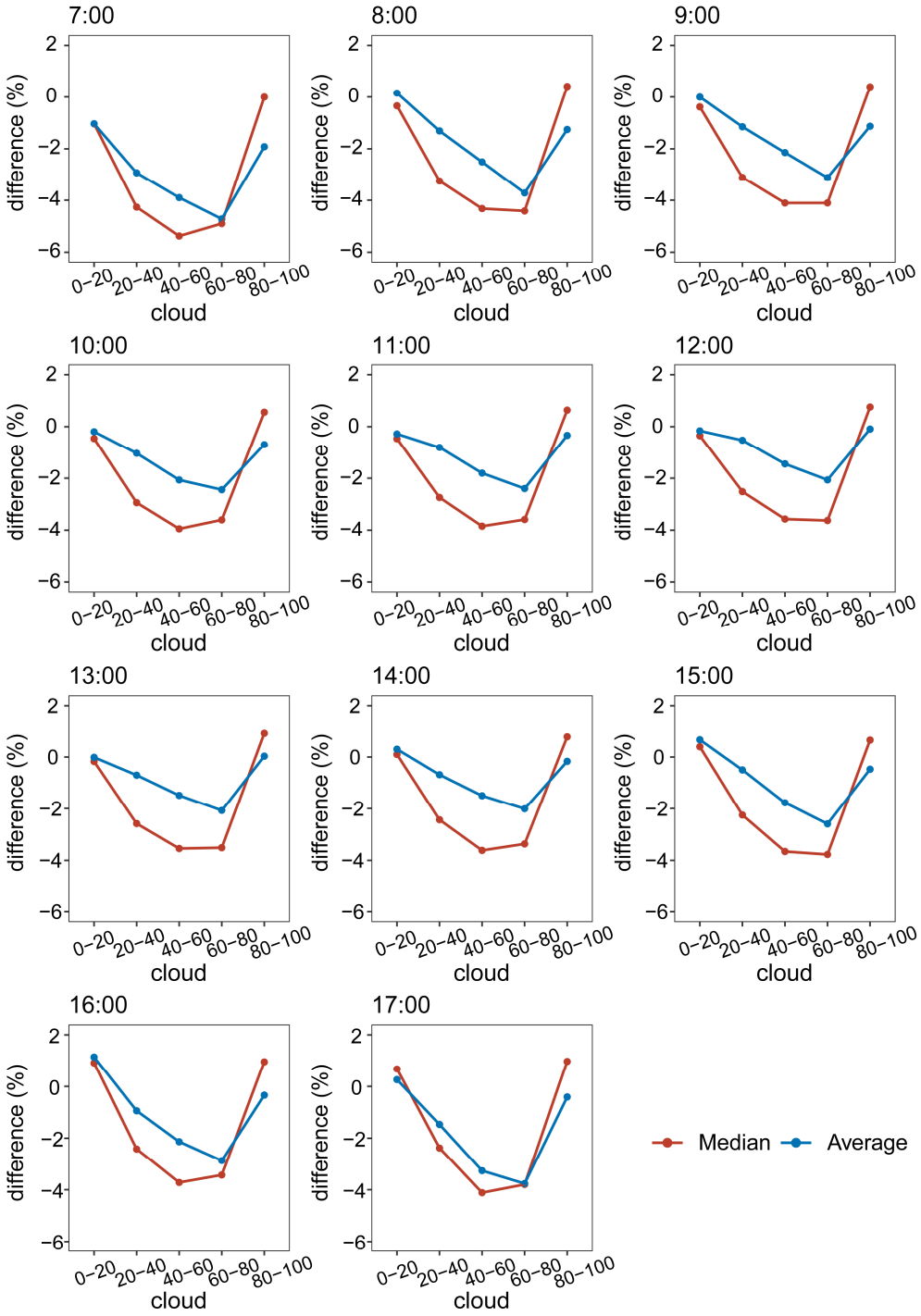

Figure 12. Median and mean values of differences between CERES and BSRN hourly R_s under different cloud cover categories from 7:00 to 17:00. The differences refer to the values that CERES data minus BSRN data.

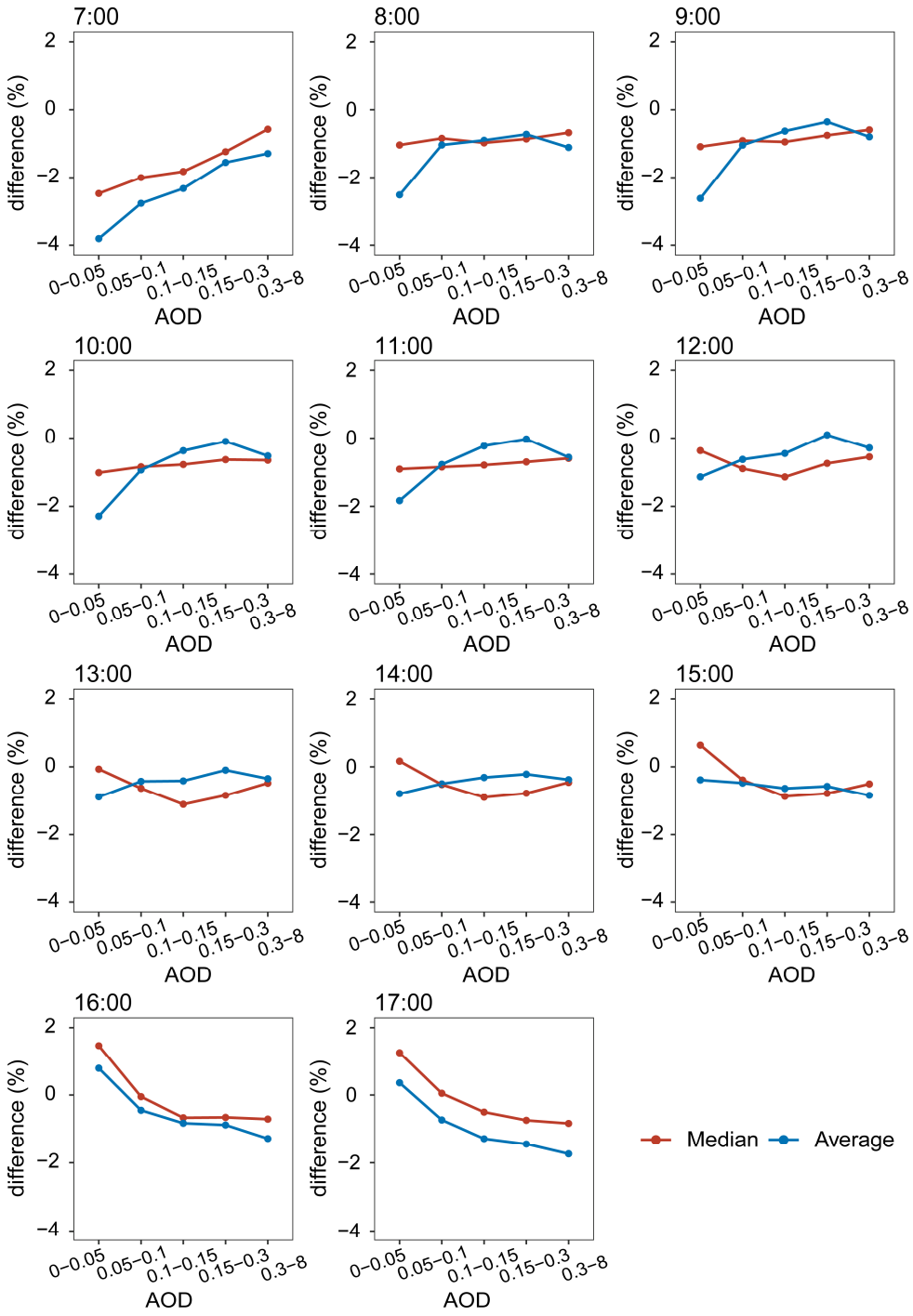

Figure 13. Median and mean values of differences between CERES and BSRN hourly R_s under different AOD categories from 7:00 to 17:00. The differences refer to the values that CERES data minus BSRN data.

Table 2. Ranges (largest bias minus smallest bias) in median Biases or average Biases (shown in Figures 12 and 13) from CERES-retrieved hourly R_s at all ground-based sites for each hour under different cloud cover and AOD conditions. Variation (the standard deviation of the biases) in the median Biases or average Biases shown in parentheses. Unit: %.

Impact Factor	Range (Variation)	7:00	8:00	9:00	10:00	11:00	12:00	13:00	14:00	15:00	16:00	17:00
cloud cover	Median Biases	5.38 (2.43)	4.83 (2.27)	4.50 (2.13)	4.51 (2.01)	4.49 (1.99)	4.39 (1.98)	4.46 (2.04)	4.39 (2.02)	4.43 (2.14)	4.68 (2.31)	5.09 (2.42)
	Average Biases	3.68 (1.48)	3.87 (1.46)	3.12 (1.18)	2.25 (0.94)	2.12 (0.94)	1.97 (0.86)	2.11 (0.92)	2.31 (0.94)	3.26 (1.27)	4.01 (1.57)	4.03 (1.75)
AOD	Median Biases	1.90 (0.74)	0.36 (0.14)	0.50 (0.19)	0.38 (0.16)	0.31 (0.12)	0.77 (0.30)	1.04 (0.39)	1.06 (0.41)	1.50 (0.60)	2.17 (0.93)	2.09 (0.86)
	Average Biases	2.52 (1.01)	1.79 (0.72)	2.27 (0.89)	2.19 (0.86)	1.80 (0.70)	1.23 (0.45)	0.79 (0.29)	0.57 (0.22)	0.46 (0.17)	2.08 (0.80)	2.10 (0.83)

For the mean, at 7:00, the negative Bias decreases significantly with increasing AOD; from 8:00 to 14:00, the negative Bias decreases with increasing AOD for the "0–0.3" range and then increases for the "0.3–8" range; from 16:00 to 17:00, the negative Bias increases with increasing AOD. The median is generally similar to the mean except for the "0–0.05" interval. AOD changes lead to a change of 0.31–2.52% and a variation of 0.12–1.01% in the R_s Biases (Table 2). The use of median and mean values derived similar results.

In general, the change in R_s Bias caused by AOD at each hour is significantly smaller than that caused by cloud cover, which in turn supports that the diurnal variation in Biases in CERES-retrieved R_s is more sensitive to cloud cover than AOD.

4. Discussion

Based on the observed R_s data at different sites in the BSRN observational network, this study evaluates CERES-retrieved hourly R_s data and explores the impact of cloud cover and AOD on the bias of CERES-retrieved R_s data. The impact of diurnal and seasonal variation on the R_s evaluation was removed by dividing the solar radiation at TOA.

The Bias, MAB and RMSE values over the continent are 2.37%, 2.36% and 2.55% smaller than those over the island/coast and polar regions, respectively, while R is 0.1 higher. This may be attributed to rapid weather changes and the presence of both land and water within the grid (edge effects) for island/coast regions, and the failure of cloud detection as more ice and snow exist for polar regions. The spatial distribution of MAB and RMSE is consistent with the results of Yang et al. [27] and Tang et al. [22]. The Bias, MAB, RMSE at 7:00 are relatively large, then decrease at midday and increase again at 17:00. R is higher at midday than at 7:00 and 17:00. The diurnal variation in R is identical to that in Hao et al. [40], but other statistical parameters are different because we removed the diurnal cycle and seasonal cycle in the R_s. MAB and RMSE for all times under clear-sky conditions are significantly 3.31–7.71% and 3.35–8.59% smaller than those under other conditions, especially around midday. Bias under clear-sky conditions is about 1.47% smaller for overcast-sky conditions (except for nearly the same at 11:00–13:00) and 2.13% smaller for cloudy-sky conditions. However, R under clear-sky conditions is lower than that under overcast-sky conditions for 9:00–15:00. R under cloudy-sky conditions is significantly lower than those under other conditions. This may be because more clouds tend to occur at midday, and during these hours, many broken clouds can easily be misjudged as clear-sky or cloudy-sky conditions. Satellites are more likely to detect circumstances under overcast-sky conditions. The change in R_s bias caused by AOD is 0.31–2.52% at all hours, which is significantly smaller than 1.97–5.38% caused by cloud cover. This is consistent with our previous studies as cloud cover drive the short-term variation in R_s and aerosols modulate its long-term variation [51,52].

5. Conclusions

Satellite-retrieved datasets have relatively high accuracy and continuity in spatial distribution compared to traditional ground-based observations and reanalyses datasets. However, the evaluations of satellite-retrieved R_s data on the diurnal scale are still lacking. In this study, CERES-retrieved R_s on the diurnal scale was evaluated by comparison with the BSRN observations during a 21-year period from 2000 to 2021, and the influence of clouds and aerosols on the diurnal variation in R_s was investigated. The findings of this study included the following:

1. CERES-retrieved R_s performs better at 11:00–13:00 (−0.55% for Bias, 8.87% for MAB, 12.58% for RMSE, and 0.84 for R) than at other hours (1.26% for Bias, 10.00% for MAB, 13.50% for RMSE, and 0.81 for R).
2. For spatial distribution, CERES-retrieved R_s performs better over the continent (−0.42% for Bias, 8.89% for MAB, 12.12% for RMSE, and 0.83 for R) than over the island/coast (−1.01% for Bias, 9.38% for MAB, 13.00% for RMSE, and 0.74 for R) and polar (−1.70% for Bias, 10.85% for MAB, 14.30% for RMSE and 0.72 for R) regions.
3. The Bias, MAB, and RMSE in CERES-retrieved R_s under clear-sky conditions are rather small, although the correlation coefficients are slightly lower than those under overcast-sky conditions from 9:00 to 15:00. R in CERES-retrieved R_s under cloudy-sky conditions are the lowest.
4. The change in R_s bias caused by cloud cover is 1.97–5.38%, significantly larger than 0.31–2.52% by AOD.

In this study, the BSRN network stations used to evaluate the hourly R_s data retrieved by CERES have a high accuracy. However, the observation quality of the BSRN station, the urbanization level of the city where the station is located, and whether there are natural or artificial factors that affect the observation near the station have not been further evaluated and discussed in detail. Additionally, in the BSRN observation network, there are many missing and null values at some stations, which makes the ground-based observation sequence discontinuous. Although some studies have shown that the accuracy of cloud covers and AOD in CERES is relatively high [45–49], further evaluation of their diurnal variations is needed. It is beyond the scope of this study but is essential for our future work.

Author Contributions: Conceptualization, Q.M.; Methodology, Q.M.; Software, L.L.; Validation, L.L. and Q.M.; Formal Analysis, Q.M.; Investigation, Q.M.; Resources, L.L.; Data Curation, L.L.; Writing—Original Draft Preparation, L.L.; Writing—Review and Editing, Q.M.; Visualization, L.L.; Supervision, Q.M. All authors have read and agreed to the published version of the manuscript.

Funding: This research was funded by National Science Foundation of China, grant number 41930970.

Data Availability Statement: Baseline Surface Radiation Network (BSRN) data are available at https://dataportals.pangaea.de/bsrn/?q=LR0100, accessed on 1 July 2021; Clouds and the Earth's Radiant Energy System for CERES SYN data are available at https://ceres.larc.nasa.gov/order_data.php, accessed on 1 July 2021.

Acknowledgments: We thank the following institutions for sharing their data freely: the NASA Langley Research Center Atmospheric Science Data Center for CERES SYN data; the World Data Center PANGAEA for BSRN observation data.

Conflicts of Interest: The authors declare no conflict of interest.

Appendix A

Table A1. The information (station name, latitude (°), longitude (°) and altitude (m)) and evaluation of CERES hourly R_s against the ground-based measurements for 53 stations. N is sample size of participating in the calculation.

Site	Lat	Long	El	Statistical Parameters	7:00	8:00	9:00	10:00	11:00	12:00	13:00	14:00	15:00	16:00	17:00
ALE (2004.08–2014.03)	−23.8	133.9	547	Bias	−2.04	−2.18	−1.69	−0.65	0.1	1.23	1.96	2.85	3.12	4.15	4.82
				MAB	11.12	11.01	10.93	10.43	9.85	9.79	9.82	9.27	9.40	9.49	9.40
				RMSE	14.21	14.39	14.29	13.58	13.28	13.18	13.17	12.31	12.61	12.56	12.35
				R	0.72	0.72	0.72	0.74	0.76	0.77	0.77	0.79	0.78	0.79	0.80
				N	1638	1715	1787	1848	1886	1912	1899	1839	1779	1709	1633
ASP (2000.03–2020.07)	71.32	−156.6	8	Bias	−1.69	−0.46	0.06	0.42	0.40	0.70	1.21	1.18	1.85	2.45	−2.20
				MAB	6.75	5.11	4.19	3.88	4.28	4.67	4.81	5.3	5.89	6.37	9.32
				RMSE	9.68	8.14	7.28	7.02	7.66	8.06	8.15	8.74	9.25	9.47	12.69
				R	0.78	0.79	0.82	0.83	0.82	0.80	0.84	0.83	0.82	0.81	0.70
				N	6709	6757	6768	6778	6775	6764	6758	6756	6752	6754	6753
BAR (2000.02–2017.08)	32.27	−64.67	8	Bias	−3.05	−3.10	−3.36	−3.37	−2.91	−1.91	−0.73	0.79	2.37	4.29	5.75
				MAB	11.18	10.87	10.27	10.12	9.69	9.36	9.16	8.96	8.99	9.45	9.86
				RMSE	14.85	14.38	13.71	13.57	12.86	12.48	12.06	11.67	11.50	11.90	12.22
				R	0.72	0.75	0.78	0.79	0.81	0.82	0.82	0.83	0.83	0.82	0.82
				N	3426	3804	4126	4381	4555	4667	4615	4448	4206	3912	3570
BER (2000.03–2017.08)	36.61	−97.52	317	Bias	−1.48	0.33	0.64	0.48	0.50	0.24	0.38	0.33	−0.57	−0.43	−1.63
				MAB	8.18	8.25	8.59	8.57	8.95	8.94	9.07	8.78	8.95	8.69	9.13
				RMSE	10.90	11.00	11.59	11.60	12.09	12.12	12.28	11.79	11.92	11.54	12.07
				R	0.81	0.81	0.78	0.77	0.76	0.76	0.76	0.77	0.77	0.78	0.73
				N	4706	4704	4697	4704	4697	4695	4697	4700	4702	4704	3994
BIL (2000.03–2019.07)	40.07	−88.37	213	Bias	−0.26	1.88	1.73	1.55	1.29	1.35	1.25	1.39	1.77	2.69	0.45
				MAB	7.75	6.30	5.75	5.58	5.46	5.63	5.46	5.66	5.92	6.84	7.76
				RMSE	11.03	8.85	8.41	8.35	8.09	8.41	8.00	8.22	8.44	9.45	10.83
				R	0.83	0.90	0.89	0.87	0.87	0.87	0.87	0.86	0.87	0.87	0.80
				N	6013	6775	6777	6779	6781	6779	6777	6780	6779	6779	5774
BON (2009.01–2020.04)	40.13	−105.2	1689	Bias	0.49	0.50	−0.94	−1.23	−1.46	−1.09	−0.81	−0.81	−0.62	0.81	2.09
				MAB	8.24	8.81	8.54	8.36	8.41	8.61	8.51	8.69	8.47	8.48	8.80
				RMSE	11.13	12.12	12.32	12.18	12.13	12.22	12.13	12.22	12.02	11.68	11.49
				R	0.83	0.85	0.86	0.87	0.86	0.86	0.86	0.85	0.85	0.86	0.86
				N	5183	7231	7240	7255	7269	7270	7270	7273	7273	7270	7164
BOS (2009.01–2020.04)	40.05	−105	1577	Bias	0.46	−0.47	−1.18	−1.48	−1.41	−1.11	−0.93	−0.47	−0.45	0.98	2.63
				MAB	10.98	10.60	10.48	10.57	11.53	11.68	12.31	12.46	12.27	11.91	11.44
				RMSE	15.33	15.03	14.89	14.67	15.69	15.71	16.32	16.37	15.95	15.25	14.55
				R	0.73	0.72	0.69	0.67	0.64	0.68	0.69	0.69	0.69	0.69	0.68
				N	7280	7315	7316	7329	7332	7333	7328	7326	7327	7347	5107
BOU (2000.02–2016.06)	−15.6	−47.71	1023	Bias	−1.77	−0.72	−1.28	−2.09	−2.75	−2.76	−2.68	−1.28	0.18	0.95	3.30
				MAB	12.31	10.88	10.29	10.28	11.23	11.59	12.29	12.30	12.28	12.14	11.50
				RMSE	16.87	15.26	14.56	14.25	15.24	15.63	16.31	16.05	15.73	15.47	14.56
				R	0.64	0.69	0.67	0.64	0.61	0.63	0.64	0.66	0.67	0.65	0.66
				N	5767	5805	5809	5830	5826	5842	5847	5846	5846	5849	4083
BRB (2006.02–2019.04)	51.97	4.93	0	Bias	−1.58	−1.00	−0.07	0.94	2.30	3.08	2.89	1.69	1.31	1.47	0.41
				MAB	7.40	6.45	6.15	6.93	8.33	9.45	10.39	10.45	10.70	10.67	10.87
				RMSE	9.82	8.92	8.99	10.06	11.88	13.18	14.18	14.17	14.29	14.24	13.90
				R	0.80	0.81	0.80	0.75	0.71	0.69	0.69	0.70	0.72	0.72	0.63
				N	3085	3086	3091	3089	3086	3083	3086	3086	3082	3084	3082
CAB (2005.02–2021.04)	50.22	−5.32	88	Bias	−2.56	−0.75	1.30	0.89	0.92	1.43	0.93	1.04	0.64	0.14	−1.47
				MAB	9.62	9.18	8.76	8.43	8.40	8.32	8.45	8.51	8.60	8.92	9.15
				RMSE	12.35	11.88	11.44	11.29	11.21	11.15	11.31	11.31	11.31	11.58	11.97
				R	0.80	0.84	0.86	0.87	0.87	0.87	0.86	0.86	0.86	0.85	0.82
				N	3939	5045	5864	5869	5866	5871	5870	5869	5871	5871	4323
CAM (2001.01–2017.07)	44.08	5.06	100	Bias	−0.16	−0.03	1.51	1.57	1.71	1.96	1.52	1.15	0.29	−0.88	−1.91
				MAB	9.36	9.45	9.32	9.62	9.82	9.91	9.61	9.48	9.15	9.46	9.61
				RMSE	12.06	12.19	12.16	12.57	12.70	12.94	12.66	12.46	11.92	12.19	12.45
				R	0.80	0.81	0.83	0.83	0.83	0.83	0.83	0.84	0.85	0.83	0.81
				N	4241	5696	5695	5696	5698	5697	5697	5697	5697	5063	3933

Table A1. *Cont.*

Site	Lat	Long	El	Statistical Parameters	7:00	8:00	9:00	10:00	11:00	12:00	13:00	14:00	15:00	16:00	17:00
CAR (2000.03–2018.12)	36.91	−75.71	37	Bias	−0.69	−0.60	−1.02	−1.53	−2.66	−2.76	−4.05	−4.70	−5.25	−6.22	−7.12
				MAB	7.72	8.55	8.84	8.89	9.05	9.11	9.87	10.30	10.94	11.29	11.75
				RMSE	10.73	11.90	12.61	12.81	12.82	12.89	13.62	14.19	15.07	15.22	15.71
				R	0.83	0.83	0.79	0.76	0.74	0.73	0.72	0.72	0.72	0.76	0.72
				N	4969	6664	6664	6663	6663	6662	6659	6658	6658	6659	5296
CLN (2000.05–2016.11)	42.82	−1.6	471	Bias	−5.33	−3.04	−2.14	−1.48	−1.84	−1.93	−2.14	−3.13	−4.91	−7.60	−9.58
				MAB	9.50	7.94	7.10	6.76	6.83	7.27	7.31	8.53	10.17	12.56	14.20
				RMSE	12.11	10.40	9.67	9.51	9.58	10.15	10.19	11.44	13.12	15.72	17.79
				R	0.86	0.88	0.88	0.88	0.87	0.87	0.87	0.85	0.82	0.78	0.66
				N	5647	5635	5619	5616	5609	5597	5605	5602	5628	5647	4069
CNR (2009.07–2021.05)	−12.19	96.84	6	Bias	2.57	4.64	4.72	4.48	4.21	4.29	2.88	3.13	2.51	−0.26	−1.59
				MAB	9.28	9.62	9.16	9.21	8.84	8.80	8.58	8.75	8.96	9.16	9.25
				RMSE	12.47	13.38	12.85	13.04	12.61	12.55	12.02	12.23	12.18	12.40	12.29
				R	0.83	0.86	0.87	0.86	0.86	0.86	0.86	0.86	0.86	0.83	0.80
				N	4083	4328	4320	4317	4317	4322	4324	4325	4332	4331	2978
COC (2004.10–2020.05)	−30.67	23.99	1287	Bias	−3.20	−0.91	−0.21	0.21	0.24	0.89	1.05	1.18	1.19	0.86	−0.21
				MAB	10.13	9.27	8.70	8.45	8.64	8.45	8.52	8.64	8.66	8.74	8.39
				RMSE	13.15	12.04	11.63	11.55	11.86	11.70	11.71	11.72	11.56	11.58	10.84
				R	0.61	0.67	0.67	0.67	0.65	0.68	0.68	0.68	0.70	0.71	0.72
				N	4209	4214	4217	4209	4197	4190	4186	4179	4172	4162	4146
DAA (2000.07–2020.01)	−12.43	130.9	30	Bias	−3.47	0.37	0.69	0.94	1.43	2.37	2.70	1.88	1.87	1.76	−1.11
				MAB	9.60	5.95	4.90	4.58	4.61	4.96	5.37	5.74	6.53	7.73	9.24
				RMSE	13.53	9.93	8.64	8.42	8.76	9.50	9.91	9.72	10.23	11.26	12.60
				R	0.75	0.81	0.80	0.79	0.78	0.78	0.80	0.79	0.76	0.75	0.77
				N	3408	3478	3503	3509	3507	3509	3513	3516	3519	3516	3506
DAR (2002.07–2015.01)	−75.1	123.4	3233	Bias	−4.08	−2.22	−1.00	1.32	1.75	1.25	1.21	1.47	−0.44	−0.37	−0.99
				MAB	8.35	7.73	7.80	8.22	9.31	9.20	8.09	7.97	7.69	7.51	7.90
				RMSE	10.93	10.47	10.71	11.91	13.10	12.92	11.99	11.82	10.99	10.75	10.56
				R	0.64	0.67	0.69	0.67	0.61	0.64	0.67	0.66	0.69	0.69	0.58
				N	4532	4533	4533	4534	4533	4533	4513	4516	4517	4517	4518
DOM (2006.01–2021.02)	36.63	−116	1007	Bias	−8.62	−11.24	−12.71	−10.59	−6.39	−5.17	−4.39	−4.74	−7.75	−6.87	−3.86
				MAB	12.50	12.54	13.60	11.68	7.79	6.73	6.22	6.76	10.12	10.43	9.27
				RMSE	16.68	16.98	18.21	15.39	10.68	9.66	9.25	9.95	14.45	15.48	13.95
				R	0.47	0.48	0.48	0.53	0.63	0.69	0.72	0.70	0.65	0.68	0.73
				N	2537	2752	2963	3101	3271	3394	3439	3378	3263	3116	2919
DRA (2009.01–2020.04)	−12.42	130.9	32	Bias	0.89	1.29	0.58	−0.56	−0.77	−0.48	−0.51	−0.31	0.63	2.27	5.03
				MAB	6.96	6.02	5.24	4.87	4.96	5.41	5.42	5.73	5.82	6.70	8.89
				RMSE	10.61	9.61	8.92	8.31	8.21	9.04	8.90	9.29	9.30	9.76	12.42
				R	0.82	0.87	0.85	0.83	0.80	0.78	0.79	0.79	0.81	0.82	0.86
				N	5692	7215	7210	7213	7214	7216	7221	7223	7223	7240	7016
DWN (2008.04–2020.07)	36.61	−97.49	318	Bias	−5.32	−2.63	−0.38	1.93	2.63	2.05	2.20	2.28	−0.52	−0.86	−2.53
				MAB	9.15	7.75	7.69	8.13	9.02	8.89	7.77	7.85	7.53	7.56	8.31
				RMSE	11.80	10.17	10.66	11.93	13.16	12.77	11.78	11.81	10.64	10.69	10.92
				R	0.64	0.67	0.69	0.67	0.59	0.61	0.66	0.66	0.68	0.70	0.60
				N	3999	4024	4025	4030	4037	4042	4041	4039	4035	4027	4026
E13 (2000.02–2019.07)	−27.6	−48.52	11	Bias	−0.59	1.58	1.42	1.12	0.76	0.84	0.72	0.86	1.20	1.99	−0.52
				MAB	7.77	6.26	5.70	5.54	5.39	5.58	5.37	5.56	5.79	6.61	7.74
				RMSE	10.99	8.76	8.34	8.30	8.01	8.36	7.89	8.14	8.30	9.26	10.89
				R	0.83	0.90	0.89	0.87	0.87	0.87	0.87	0.87	0.87	0.87	0.80
				N	6125	6884	6894	6890	6892	6893	6894	6893	6892	6892	5987
FLO (2000.04–2021.03)	48.32	−105.1	634	Bias	0.13	0.00	0.30	−0.14	0.51	0.19	−0.45	−1.38	−0.59	−0.57	0.25
				MAB	8.91	8.72	8.56	8.42	8.27	8.10	8.45	8.86	9.02	9.21	8.88
				RMSE	11.67	11.62	11.69	11.45	11.38	10.93	11.32	11.75	12.24	12.37	12.08
				R	0.81	0.85	0.86	0.86	0.86	0.87	0.86	0.86	0.85	0.83	0.72
				N	4485	4501	4509	4510	4509	4508	4510	4509	4495	4476	4470
FPE (2009.01–2020.05)	33.58	130.4	3	Bias	1.26	1.21	0.06	0.56	0.69	0.48	0.00	−0.79	0.48	2.31	3.33
				MAB	9.00	8.94	8.73	8.02	8.02	8.27	8.60	9.08	9.41	9.77	9.90
				RMSE	12.50	12.49	12.46	11.47	11.35	11.66	11.99	12.61	12.76	13.07	13.05
				R	0.83	0.84	0.82	0.83	0.82	0.81	0.80	0.80	0.80	0.79	0.76
				N	5631	6701	6735	6737	6747	6758	6778	6775	6746	5694	4363

Table A1. *Cont.*

Site	Lat	Long	El	Statistical Parameters	7:00	8:00	9:00	10:00	11:00	12:00	13:00	14:00	15:00	16:00	17:00
FUA (2010.04–2021.04)	34.25	−89.87	98	Bias	−0.76	0.71	0.62	0.55	0.61	0.75	0.80	0.40	−0.01	0.21	−2.24
				MAB	7.40	7.22	7.20	7.38	7.66	7.88	7.71	7.55	7.48	7.59	8.10
				RMSE	9.61	9.58	9.74	10.03	10.36	10.55	10.44	10.21	9.96	10.06	10.67
				R	0.88	0.91	0.91	0.90	0.90	0.90	0.90	0.90	0.90	0.89	0.84
				N	4014	4013	4013	4012	4010	4007	4010	4010	4012	4014	3232
GCR (2009.01–2020.04)	−23.56	15.04	407	Bias	3.19	3.02	1.92	1.09	0.73	0.63	0.51	0.08	0.02	0.68	1.21
				MAB	7.35	7.44	6.54	5.94	6.13	6.45	6.63	6.95	7.17	7.54	8.40
				RMSE	9.58	9.92	8.92	8.37	8.71	9.08	9.45	9.85	10.08	10.42	11.35
				R	0.86	0.89	0.89	0.90	0.90	0.89	0.89	0.88	0.85	0.85	0.83
				N	5285	7093	7158	7203	7203	7204	7206	7205	7205	7193	7150
GOB (2012.05–2021.04)	−70.65	−8.25	42	Bias	2.00	4.00	1.26	1.09	0.75	0.35	0.62	−0.29	−1.54	−4.38	−7.75
				MAB	13.91	10.98	7.23	4.31	2.94	2.59	2.49	2.76	3.54	6.06	9.20
				RMSE	17.39	15.50	11.52	7.94	5.76	5.01	4.92	5.36	5.91	8.66	11.82
				R	0.33	0.53	0.70	0.78	0.78	0.73	0.76	0.78	0.70	0.62	0.66
				N	2903	3211	3213	3214	3214	3213	3213	3213	3215	3215	3214
GVN (2000.03–2021.01)	24.34	124.2	5.7	Bias	−13.25	−13.34	−13.45	−12.15	−10.83	−8.67	−8.06	−6.71	−4.80	−2.66	−1.34
				MAB	16.68	16.30	16.19	15.01	14.06	12.60	12.24	11.54	10.94	10.45	10.06
				RMSE	20.97	20.40	20.02	18.69	17.87	16.05	15.84	14.85	14.17	13.64	13.21
				R	0.54	0.59	0.62	0.65	0.67	0.70	0.70	0.72	0.71	0.70	0.70
				N	3831	4381	4963	5365	5736	5925	5942	5640	5298	4860	4364
ISH (2010.04–2021.04)	28.31	−16.5	2372.9	Bias	−1.25	−0.85	−0.55	−0.27	0.44	0.86	1.16	0.94	−0.23	−1.18	−2.66
				MAB	7.12	7.45	7.57	8.11	8.09	8.56	8.72	8.67	8.65	8.44	8.66
				RMSE	9.51	10.03	10.27	11.10	11.19	11.92	12.15	12.05	11.74	11.35	11.56
				R	0.85	0.87	0.87	0.85	0.84	0.83	0.83	0.83	0.84	0.85	0.84
				N	4009	4007	4006	4003	4006	4006	4004	4005	4006	4008	4008
IZA (2009.03–2021.06)	8.72	167.7	10	Bias	−25.76	−22.14	−19.26	−16.82	−15.28	−14.21	−14.72	−14.97	−17.67	−22.17	−27.90
				MAB	26.60	23.36	20.91	19.26	18.60	18.26	18.57	18.81	21.04	24.55	28.93
				RMSE	28.98	25.83	23.43	21.68	20.80	20.51	20.85	21.01	23.24	26.93	31.66
				R	0.48	0.24	0.19	0.19	0.22	0.23	0.26	0.34	0.39	0.53	0.52
				N	4441	4435	4439	4442	4445	4444	4443	4441	4444	4447	3662
KWA (2000.03–2017.08)	−45.05	169.7	350	Bias	−3.74	−0.82	−0.49	−0.31	−0.34	−0.95	−0.24	−0.02	0.91	0.77	1.11
				MAB	10.12	9.11	8.62	8.13	8.06	8.56	8.13	8.12	7.97	7.76	7.75
				RMSE	13.09	12.08	11.60	11.19	11.14	11.78	11.17	11.20	10.91	10.44	10.22
				R	0.55	0.67	0.71	0.72	0.71	0.71	0.72	0.74	0.74	0.75	0.75
				N	5945	5934	5872	5669	5585	5480	5596	5645	5904	5958	5965
LAU (2000.03–2018.12)	60.14	−1.18	80	Bias	−7.58	−7.80	−5.14	−4.02	−3.64	−3.58	−3.14	−3.10	−3.35	−1.59	−1.00
				MAB	15.93	16.05	14.44	13.59	13.66	13.28	13.05	13.10	13.22	12.14	11.38
				RMSE	20.59	21.00	18.30	17.25	17.53	17.24	17.06	17.18	17.43	16.07	15.02
				R	0.57	0.58	0.68	0.69	0.67	0.68	0.68	0.68	0.67	0.69	0.70
				N	4319	6132	6319	6364	6391	6413	6411	6409	6411	6420	5318
LER (2001.01–2017.07)	52.21	14.12	125	Bias	0.12	−0.63	−1.74	−1.01	−1.18	−0.48	−0.27	−0.54	0.58	1.42	2.20
				MAB	11.42	11.30	11.46	10.85	10.73	10.71	10.80	11.50	11.69	11.67	11.60
				RMSE	14.13	14.24	14.86	13.92	13.87	13.73	13.80	14.69	14.83	14.66	14.34
				R	0.71	0.74	0.73	0.78	0.78	0.79	0.78	0.73	0.72	0.69	0.66
				N	3748	4378	5375	5378	5380	5379	5381	5381	4484	3872	3235
LIN (2000.03–2018.12)	−2.06	147.4	6	Bias	−1.67	−1.50	−1.11	−1.96	−1.77	−1.67	−2.20	−2.38	−3.57	−5.05	−6.92
				MAB	8.81	9.19	9.22	9.09	9.23	9.35	9.56	9.58	10.69	11.22	12.20
				RMSE	11.24	11.93	12.09	12.10	12.08	12.43	12.67	12.73	14.04	14.67	15.58
				R	0.86	0.85	0.86	0.86	0.86	0.85	0.84	0.83	0.79	0.75	0.70
				N	3035	3893	3892	3894	3893	3893	3893	3894	3894	3031	2418
LRC (2014.12–2021.05)	24.29	154	7.1	Bias	−3.87	−2.66	−1.69	−1.04	−0.27	0.69	1.75	1.99	1.58	−0.50	−2.30
				MAB	10.37	10.23	10.20	11.03	11.68	12.39	12.56	12.24	11.67	10.83	9.78
				RMSE	13.23	13.20	13.41	14.57	15.36	16.17	16.60	16.18	15.21	13.95	12.56
				R	0.70	0.73	0.73	0.71	0.71	0.70	0.68	0.69	0.70	0.69	0.60
				N	4887	4891	4896	4889	4890	4889	4889	4890	4888	4886	4886
MAN (2000.03–2013.10)	−0.52	166.9	7	Bias	−8.90	−3.62	−1.82	−0.69	0.04	0.36	0.37	0.63	0.23	−0.71	−0.93
				MAB	12.74	9.55	8.39	7.47	7.16	7.32	7.02	7.20	7.28	7.36	7.07
				RMSE	16.46	12.61	11.50	10.67	10.63	10.91	10.46	10.54	10.32	10.10	9.37
				R	0.58	0.70	0.71	0.70	0.71	0.69	0.71	0.72	0.74	0.76	0.82
				N	3975	3976	3977	3975	3969	3964	3958	3954	3959	3966	3972

Table A1. *Cont.*

Site	Lat	Long	El	Statistical Parameters	7:00	8:00	9:00	10:00	11:00	12:00	13:00	14:00	15:00	16:00	17:00
MNM (2010.04–2021.04)	78.93	11.93	11	Bias	−4.64	−1.01	−0.46	0.72	1.76	2.44	3.48	3.96	4.38	4.23	2.99
				MAB	9.36	8.13	7.75	7.90	8.39	8.67	9.24	9.50	9.53	9.36	8.97
				RMSE	12.23	11.01	10.82	11.52	12.45	12.69	13.33	13.50	13.12	12.55	11.77
				R	0.55	0.64	0.61	0.59	0.57	0.56	0.55	0.55	0.58	0.60	0.63
				N	4857	4860	4861	4865	4863	4866	4869	4865	4864	4865	4866
NAU (2000.03–2013.09)	48.71	2.21	156	Bias	−9.97	−8.79	−7.43	−6.45	−4.67	−3.18	−1.93	−2.12	−3.84	−3.68	−3.65
				MAB	15.22	14.25	13.62	13.03	12.23	11.96	12.06	11.21	10.99	10.79	10.75
				RMSE	20.03	18.54	17.48	16.88	15.94	15.71	15.79	14.58	14.45	14.19	14.09
				R	0.60	0.64	0.67	0.68	0.69	0.68	0.64	0.70	0.73	0.73	0.72
				N	4299	4601	4864	5057	5183	5267	5200	5040	4839	4579	4278
NYA (2000.03–2021.07)	46.82	6.94	491	Bias	−0.65	0.77	2.35	1.87	1.21	1.08	0.66	0.43	0.47	−0.24	−2.34
				MAB	8.23	8.52	8.74	8.18	8.64	8.67	9.04	8.87	9.16	9.69	10.09
				RMSE	10.66	11.31	11.74	11.11	11.62	11.45	12.00	11.74	12.10	12.58	13.12
				R	0.85	0.86	0.87	0.88	0.86	0.87	0.85	0.86	0.84	0.81	0.77
				N	3363	4435	4997	5000	5003	5001	5001	4998	4996	4995	3950
PAL (2005.10–2019.12)	40.72	−77.93	376	Bias	1.39	3.31	3.28	2.72	1.89	2.01	0.74	0.66	0.72	0.41	−1.12
				MAB	9.26	10.38	10.89	10.67	10.74	10.37	10.23	10.25	10.20	10.05	9.51
				RMSE	12.25	13.81	14.78	14.71	14.66	14.23	13.86	13.84	13.67	13.13	12.56
				R	0.83	0.81	0.80	0.80	0.79	0.80	0.80	0.80	0.81	0.82	0.81
				N	5548	7500	7497	7497	7496	7503	7502	7505	7508	7507	5674
PAY (2000.03–2020.12)	−9.07	−40.32	387	Bias	4.79	2.61	2.16	1.59	1.45	1.26	0.74	0.53	0.71	1.23	0.51
				MAB	9.37	8.17	8.20	8.13	8.40	8.62	8.63	8.57	8.76	9.10	9.36
				RMSE	12.08	11.25	11.37	11.28	11.51	11.80	11.82	11.73	11.76	12.05	12.38
				R	0.85	0.88	0.89	0.89	0.88	0.88	0.87	0.87	0.86	0.84	0.78
				N	7244	7228	7223	7228	7226	7227	7232	7230	7232	7225	5216
PSU (2009.01–2020.04)	50.21	−104.7	578	Bias	1.41	2.98	4.36	5.07	5.09	4.62	3.50	2.36	1.75	0.88	2.49
				MAB	9.26	9.56	9.53	9.17	8.70	8.36	7.87	7.66	7.82	7.96	8.27
				RMSE	11.96	12.49	12.37	11.99	11.40	10.89	10.24	10.01	10.31	10.53	11.32
				R	0.64	0.69	0.71	0.73	0.73	0.73	0.69	0.66	0.64	0.63	0.61
				N	3246	3275	3286	3287	3289	3287	3285	3284	3289	3288	3287
PTR (2006.12–2018.07)	43.06	141.3	17.2	Bias	−6.64	−5.18	−4.08	−3.52	−2.97	−2.30	−2.61	−2.87	−3.85	−2.54	−1.69
				MAB	12.54	11.56	10.90	9.94	9.23	8.98	9.27	9.78	10.26	9.44	9.09
				RMSE	16.30	15.70	14.78	13.87	13.01	12.67	13.30	13.88	14.62	13.28	12.58
				R	0.72	0.74	0.77	0.80	0.81	0.81	0.79	0.78	0.78	0.79	0.78
				N	2705	3448	4277	4289	4298	4304	4307	4307	4308	4306	3471
REG (2000.02–2011.12)	30.86	34.78	500	Bias	−5.96	−7.76	−7.38	−6.64	−5.81	−4.25	−3.80	−3.64	−3.97	−4.46	−4.29
				MAB	11.81	13.33	13.67	13.54	13.57	13.14	13.04	12.92	12.51	11.70	10.83
				RMSE	15.19	17.51	18.16	18.13	18.28	17.74	17.59	17.56	16.99	15.75	14.29
				R	0.72	0.68	0.68	0.68	0.66	0.66	0.67	0.67	0.68	0.69	0.72
				N	3024	3872	3873	3875	3872	3875	3875	3873	3873	3878	3089
SAP (2010.04–2020.11)	−29.44	−53.82	489	Bias	1.76	2.84	2.51	2.40	1.87	2.44	2.20	2.47	3.46	4.87	7.86
				MAB	7.35	6.08	5.46	4.85	4.45	4.31	4.33	4.68	5.25	6.39	8.89
				RMSE	10.07	8.99	8.61	8.00	7.45	7.63	7.47	7.85	8.28	8.95	11.80
				R	0.80	0.83	0.81	0.81	0.82	0.82	0.84	0.85	0.88	0.89	0.92
				N	3169	3472	3469	3474	3469	3468	3471	3472	3474	3471	3469
SBO (2003.01–2012.12)	47.05	12.96	3108.9	Bias	−3.09	−2.04	−2.26	−1.66	−0.68	0.28	0.77	−0.43	−0.76	−1.67	−4.34
				MAB	8.19	7.24	6.82	6.27	6.38	6.71	7.07	7.22	7.41	7.71	9.12
				RMSE	10.64	9.76	9.41	8.93	9.23	9.92	10.34	10.35	10.66	10.87	12.17
				R	0.89	0.91	0.91	0.91	0.90	0.89	0.89	0.88	0.87	0.88	0.86
				N	3757	3759	3759	3758	3759	3758	3759	3761	3761	3762	3762
SMS (2006.04–2017.06)	−89.98	−24.8	2800	Bias	−15.77	−15.15	−15.26	−13.77	−12.10	−9.58	−8.98	−7.89	−7.96	−8.05	−7.42
				MAB	19.60	19.07	19.73	19.54	19.27	19.16	19.44	18.76	18.11	17.80	16.64
				RMSE	23.91	23.22	23.56	23.54	23.25	23.13	23.44	22.89	22.11	22.01	20.80
				R	0.68	0.67	0.64	0.60	0.58	0.53	0.50	0.49	0.50	0.48	0.49
				N	2330	2885	2882	2855	2854	2868	2866	2888	2917	2605	1959
SPO (2000.02–2017.03)	43.73	−96.62	473	Bias	−4.56	−5.83	−6.66	−7.01	−6.80	−6.11	−5.08	−3.81	−2.83	−1.51	−0.22
				MAB	8.32	9.07	9.39	9.64	9.31	8.90	8.40	7.58	7.47	7.46	7.71
				RMSE	11.18	12.09	12.44	12.79	12.51	11.95	11.39	10.12	10.09	9.90	10.12
				R	0.70	0.69	0.69	0.68	0.70	0.71	0.73	0.76	0.75	0.76	0.75
				N	2800	2794	2771	2762	2719	2733	2752	2756	2773	2807	2824

Table A1. *Cont.*

Site	Lat	Long	El	Statistical Parameters	7:00	8:00	9:00	10:00	11:00	12:00	13:00	14:00	15:00	16:00	17:00
SXF (2009.01–2019.11)	−69.01	39.59	18	Bias	3.39	2.54	0.75	1.28	1.36	1.35	1.45	1.25	1.35	2.73	2.54
				MAB	8.53	8.74	8.24	7.63	7.48	7.38	7.46	7.82	8.29	8.69	8.69
				RMSE	11.56	12.37	12.08	11.14	11.02	10.77	10.95	11.38	11.90	11.93	11.80
				R	0.86	0.85	0.85	0.86	0.86	0.86	0.86	0.85	0.85	0.85	0.83
				N	4786	5916	5932	5933	5942	5946	5943	5936	5940	5938	4538
SYO (2000.03–2021.04)	22.79	5.53	1385	Bias	6.69	5.49	4.67	4.28	4.73	5.29	5.64	5.84	6.88	8.52	9.45
				MAB	13.64	12.90	12.58	12.61	12.57	12.22	12.21	11.99	12.46	12.58	13.16
				RMSE	18.31	17.71	17.34	17.26	17.13	16.76	16.78	16.68	17.21	17.30	17.59
				R	0.60	0.62	0.64	0.65	0.66	0.69	0.69	0.69	0.68	0.70	0.69
				N	4084	4616	5065	5456	5756	5910	5783	5455	5068	4586	4063
TAM (2000.03–2021.06)	36.06	140.1	25	Bias	−4.23	−3.37	−3.02	−2.54	−2.50	−2.31	−0.73	0.67	1.23	0.46	0.28
				MAB	7.02	5.76	5.13	4.98	5.28	6.04	6.48	6.95	7.33	7.96	7.96
				RMSE	9.02	7.61	6.85	6.86	7.24	8.39	9.73	10.70	11.19	11.21	10.73
				R	0.76	0.74	0.72	0.67	0.62	0.65	0.72	0.77	0.80	0.79	0.76
				N	7298	7314	7318	7322	7324	7321	7326	7324	7326	7323	7323
TAT (2000.03–2021.05)	58.25	26.46	70	Bias	−1.54	0.13	0.59	0.89	1.02	0.48	−0.14	−1.15	−1.99	−2.88	−6.33
				MAB	8.85	7.96	7.64	7.42	7.64	8.44	8.40	8.73	8.94	9.36	11.96
				RMSE	11.69	10.62	10.52	10.25	10.42	11.33	11.15	11.50	11.75	12.19	16.18
				R	0.79	0.86	0.88	0.89	0.88	0.86	0.85	0.84	0.84	0.83	0.70
				N	6443	7725	7727	7726	7726	7724	7725	7724	7723	7724	7246
TOR (2000.03–2020.11)	39.75	117	32	Bias	−1.07	−1.11	−1.06	−0.41	−0.75	−0.49	−0.20	0.01	−0.86	−1.32	−2.18
				MAB	10.58	10.07	9.40	8.57	8.55	8.82	8.98	9.74	10.71	11.18	11.41
				RMSE	13.45	13.05	12.37	11.36	11.30	11.67	11.84	12.64	13.93	14.34	14.33
				R	0.80	0.84	0.85	0.88	0.88	0.87	0.87	0.84	0.79	0.75	0.72
				N	5263	6247	7567	7567	7564	7569	7569	7571	6750	5657	4735
XIA (2005.01–2015.10)	82.49	−62.42	127	Bias	−1.60	2.07	2.34	2.27	1.60	−2.43	−2.01	−2.23	−1.61	−1.21	−1.65
				MAB	8.93	7.53	7.35	6.96	6.62	6.72	6.59	6.84	7.09	6.83	6.79
				RMSE	11.67	10.07	10.06	9.53	9.15	9.04	8.87	8.98	9.17	8.83	8.87
				R	0.78	0.87	0.88	0.88	0.88	0.90	0.90	0.89	0.87	0.87	0.84
				N	3635	3650	3650	3650	3651	3651	3652	3653	3653	3653	2784

References

1. Zhao, R.Z.; Wang, K.C.; Wu, G.C.; Zhou, C.L. Temperature annual cycle variations and responses to surface solar radiation in China between 1960 and 2016. *Int. J. Climatol.* **2021**, *41*, E2959–E2978. [CrossRef]
2. Kodera, K.; Kuroda, Y. Dynamical response to the solar cycle. *J. Geophys. Res. Atmos.* **2002**, *107*, 4749. [CrossRef]
3. Papaioannou, G.; Kitsara, G.; Athanasatos, S. Impact of global dimming and brightening on reference evapotranspiration in Greece. *J. Geophys. Res. Atmos.* **2011**, *116*, D9. [CrossRef]
4. Robock, A. Forty-five years of observed soil moisture in the Ukraine: No summer desiccation (yet). *Geophys. Res. Lett.* **2005**, *32*, L03401. [CrossRef]
5. Pellicciotti, F.; Brock, B.; Strasser, U.; Burlando, P.; Funk, M.; Corripio, J. An enhanced temperature-index glacier melt model including the shortwave radiation balance: Development and testing for Haut Glacier d'Arolla, Switzerland. *J. Glaciol.* **2005**, *51*, 573–587. [CrossRef]
6. Wild, M.; Trüssel, B.; Ohmura, A.; Long, C.N.; König-Langlo, G.; Dutton, E.G.; Tsvetkov, A. Global dimming and brightening: An update beyond 2000. *J. Geophys. Res. Atmos.* **2009**, *114*, D10. [CrossRef]
7. Ballare, C.L.; Caldwell, M.M.; Flint, S.D.; Robinson, A.; Bornman, J.F. Effects of solar ultraviolet radiation on terrestrial ecosystems. Patterns, mechanisms, and interactions with climate change. *Photochem. Photobiol. Sci.* **2011**, *10*, 226–241. [CrossRef]
8. Caldwell, M.M.; Bornman, J.F.; Ballare, C.L.; Flint, S.D.; Kulandaivelu, G. Terrestrial ecosystems, increased solar ultraviolet radiation, and interactions with other climate change factors. *Photochem. Photobiol. Sci.* **2007**, *6*, 252–266. [CrossRef]
9. Korany, M.; Boraiy, M.; Eissa, Y.; Aoun, Y.; Abdel Wahab, M.M.; Alfaro, S.C.; Blanc, P.; El-Metwally, M.; Ghedira, H.; Hungershoefer, K.; et al. A database of multi-year (2004–2010) quality-assured surface solar hourly irradiation measurements for the Egyptian territory. *Earth Syst. Sci. Data* **2016**, *8*, 105–113. [CrossRef]
10. Wang, K.; Dickinson, R.E.; Ma, Q.; Augustine, J.A.; Wild, M. Measurement Methods Affect the Observed Global Dimming and Brightening. *J. Clim.* **2013**, *26*, 4112–4120. [CrossRef]
11. Allen, R.J.; Norris, J.R.; Wild, M. Evaluation of multidecadal variability in CMIP5 surface solar radiation and inferred underestimation of aerosol direct effects over Europe, China, Japan, and India. *J. Geophys. Res. Atmos.* **2013**, *118*, 6311–6336. [CrossRef]
12. Xia, X. A closer looking at dimming and brightening in China during 1961–2005. *Ann. Geophys.* **2010**, *28*, 1121–1132. [CrossRef]

13. Obregón, M.Á.; Serrano, A.; Costa, M.J.; Silva, A.M. Global Spatial and Temporal Variation of the Combined Effect of Aerosol and Water Vapour on Solar Radiation. *Remote Sens.* **2021**, *13*, 708. [CrossRef]
14. Wang, K.; Ma, Q.; Li, Z.; Wang, J. Decadal variability of surface incident solar radiation over China: Observations, satellite retrievals, and reanalyses. *J. Geophys. Res. Atmos.* **2015**, *120*, 6500–6514. [CrossRef]
15. Li, J.; You, Q.; He, B. Distinctive spring shortwave cloud radiative effect and its inter-annual variation over southeastern China. *Atmos. Sci. Lett.* **2020**, *21*, e970. [CrossRef]
16. Wang, Y.; Lyu, R.; Xie, X.; Meng, Z.; Huang, M.; Wu, J.; Mu, H.; Yu, Q.R.; He, Q.; Cheng, T. Retrieval of gridded aerosol direct radiative forcing based on multiplatform datasets. *Atmos. Meas. Tech.* **2020**, *13*, 575–592. [CrossRef]
17. Zhang, Y.; Long, C.N.; Rossow, W.B.; Dutton, E.G. Exploiting diurnal variations to evaluate the ISCCP-FD flux calculations and radiative-flux-analysis-processed surface observations from BSRN, ARM, and SURFRAD. *J. Geophys. Res.* **2010**, *115*, D15. [CrossRef]
18. Ye, J.; Li, F.; Sun, G.; Guo, A. Solar dimming and its impact on estimating solar radiation from diurnal temperature range in China, 1961–2007. *Theor. Appl. Climatol.* **2010**, *101*, 137–142. [CrossRef]
19. Du, J.; Wang, K.; Wang, J.; Jiang, S.; Zhou, C. Diurnal Cycle of Surface Air Temperature within China in Current Reanalyses: Evaluation and Diagnostics. *J. Clim.* **2018**, *31*, 4585–4603. [CrossRef]
20. Shinoda, T. Impact of the Diurnal Cycle of Solar Radiation on Intraseasonal SST Variability in the Western Equatorial Pacific. *J. Clim.* **2005**, *18*, 2628–2636. [CrossRef]
21. Zhou, S.; Ma, Y.; Ge, X. Impacts of the Diurnal Cycle of Solar Radiation on Spiral Rainbands. *Adv. Atmos. Sci.* **2016**, *33*, 1085–1095. [CrossRef]
22. Tang, W.; Yang, K.; Qin, J.; Li, X.; Niu, X. A 16-year dataset (2000–2015) of high-resolution (3 h, 10 km) global surface solar radiation. *Earth Syst. Sci. Data* **2019**, *11*, 1905–1915. [CrossRef]
23. Jiang, H.; Lu, N.; Qin, J.; Yao, L. Hourly 5-km surface total and diffuse solar radiation in China, 2007–2018. *Sci. Data* **2020**, *7*, 311. [CrossRef] [PubMed]
24. Letu, H.; Nakajima, T.Y.; Wang, T.; Shang, H.; Ma, R.; Yang, K.; Baran, A.J.; Riedi, J.; Ishimoto, H.; Yoshida, M.; et al. A New Benchmark for Surface Radiation Products over the East Asia–Pacific Region Retrieved from the Himawari-8/AHI Next-Generation Geostationary Satellite. *Bull. Am. Meteorol. Soc.* **2022**, *103*, E873–E888. [CrossRef]
25. He, Y.; Wang, K.; Feng, F. Improvement of ERA5 over ERA-Interim in Simulating Surface Incident Solar Radiation throughout China. *J. Clim.* **2021**, *34*, 3853–3867. [CrossRef]
26. Träger-Chatterjee, C.; Müller, R.W.; Trentmann, J.; Bendix, J. Evaluation of ERA-40 and ERA-interim re-analysis incoming surface shortwave radiation datasets with mesoscale remote sensing data. *Meteorol. Z.* **2010**, *19*, 631–640. [CrossRef]
27. Yang, D.; Bright, J.M. Worldwide validation of 8 satellite-derived and reanalysis solar radiation products: A preliminary evaluation and overall metrics for hourly data over 27 years. *Sol. Energy* **2020**, *210*, 3–19. [CrossRef]
28. Ma, Q.; Wang, K.; Wild, M. Impact of geolocations of validation data on the evaluation of surface incident shortwave radiation from Earth System Models. *J. Geophys. Res. Atmos.* **2015**, *120*, 6825–6844. [CrossRef]
29. White, J.W.; Hoogenboom, G.; Wilkens, P.W.; Stackhouse, P.W., Jr.; Hoel, J.M. Evaluation of Satellite-Based, Modeled-Derived Daily Solar Radiation Data for the Continental United States. *Agron. J.* **2011**, *103*, 1242–1251. [CrossRef]
30. Driemel, A.; Augustine, J.; Behrens, K.; Colle, S.; Cox, C.; Cuevas-Agullo, E.; Denn, F.M.; Duprat, T.; Fukuda, M.; Grobe, H.; et al. Baseline Surface Radiation Network (BSRN): Structure and data description (1992–2017). *Earth Syst. Sci. Data* **2018**, *10*, 1491–1501. [CrossRef]
31. Tang, W.; Qin, J.; Yang, K.; Zhu, F.; Zhou, X. Does ERA5 outperform satellite products in estimating atmospheric downward longwave radiation at the surface? *Atmos. Res.* **2021**, *252*, 105453. [CrossRef]
32. Dutton, E.G.; Michalsky, J.J.; Stoffel, T.; Forgan, B.W.; Hickey, J.; Nelson, D.W.; Alberta, T.L.; Reda, I. Measurement of Broadband Diffuse Solar Irradiance Using Current Commercial Instrumentation with a Correction for Thermal Offset Errors. *J. Atmos. Ocean. Technol.* **2001**, *18*, 297–314. [CrossRef]
33. Wielicki, B.A.; Barkstrom, B.R.; Harrison, E.F.; Lee, R.B.; Smith, G.L.; Cooper, J.E. Clouds and the Earth's Radiant Energy System (CERES): An Earth Observing System Experiment. *Bull. Am. Meteorol. Soc.* **1996**, *77*, 853–868. [CrossRef]
34. Trepte, Q.Z.; Minnis, P.; Sun-Mack, S.; Yost, C.R.; Chen, Y.; Jin, Z.H.; Hong, G.; Chang, F.L.; Smith, W.L.; Bedka, K.M.; et al. Global Cloud Detection for CERES Edition 4 Using Terra and Aqua MODIS Data. *IEEE Trans. Geosci. Remote Sens.* **2019**, *57*, 9410–9449. [CrossRef]
35. Rutan, D.A.; Kato, S.; Doelling, D.R.; Rose, F.G.; Nguyen, L.T.; Caldwell, T.E.; Loeb, N.G. CERES Synoptic Product: Methodology and Validation of Surface Radiant Flux. *J. Atmos. Ocean. Technol.* **2015**, *32*, 1121–1143. [CrossRef]
36. Kratz, D.P.; Rose, F.G. Accounting for molecular absorption within the spectral range of the CERES window channel. *J. Quant. Spectrosc. Radiat. Transf.* **1999**, *61*, 83–95. [CrossRef]
37. Collins, W.D.; Rasch, P.J.; Eaton, B.E.; Khattatov, B.V.; Lamarque, J.-F.; Zender, C.S. Simulating aerosols using a chemical transport model with assimilation of satellite aerosol retrievals: Methodology for INDOEX. *J. Geophys. Res. Atmos.* **2001**, *106*, 7313–7336. [CrossRef]
38. Loeb, N.G.; Doelling, D.R.; Wang, H.; Su, W.; Nguyen, C.; Corbett, J.G.; Liang, L.; Mitrescu, C.; Rose, F.G.; Kato, S. Clouds and the Earth's Radiant Energy System (CERES) Energy Balanced and Filled (EBAF) Top-of-Atmosphere (TOA) Edition-4.0 Data Product. *J. Clim.* **2018**, *31*, 895–918. [CrossRef]

39. García, R.D.; Cuevas, E.; Ramos, R.; Cachorro, V.E.; Redondas, A.; Moreno-Ruiz, J.A. Description of the Baseline Surface Radiation Network (BSRN) station at the Izaña Observatory (2009–2017): Measurements and quality control/assurance procedures. *Geosci. Instrum. Method Data Syst.* **2019**, *8*, 77–96. [CrossRef]
40. Hao, D.; Asrar, G.R.; Zeng, Y.; Zhu, Q.; Wen, J.; Xiao, Q.; Chen, M. DSCOVR/EPIC-derived global hourly and daily downward shortwave and photosynthetically active radiation data at $0.1^\circ \times 0.1^\circ$ resolution. *Earth Syst. Sci. Data* **2020**, *12*, 2209–2221. [CrossRef]
41. Urraca, R.; Huld, T.; Gracia-Amillo, A.; Martinez-de-Pison, F.J.; Kaspar, F.; Sanz-Garcia, A. Evaluation of global horizontal irradiance estimates from ERA5 and COSMO-REA6 reanalyses using ground and satellite-based data. *Sol. Energy* **2018**, *164*, 339–354. [CrossRef]
42. Boland, J.; David, M.; Lauret, P. Short term solar radiation forecasting: Island versus continental sites. *Energy* **2016**, *113*, 186–192. [CrossRef]
43. Wang, H.; Pinker, R.T. Shortwave radiative fluxes from MODIS: Model development and implementation. *J. Geophys. Res. Atmos.* **2009**, *114*, D19. [CrossRef]
44. Redemann, J.W.; Wood, R.; Zuidema, P.; Doherty, S.J.; Luna, B.; LeBlanc, S.E.; Diamond, M.S.; Shinozuka, Y.; Chang, I.Y.; Ueyama, R.; et al. An overview of the ORACLES (ObseRvations of Aerosols above CLouds and their intEractionS) project: Aerosol–cloud–radiation interactions in the southeast Atlantic basin. *Atmos. Chem. Phys.* **2021**, *21*, 1507–1563. [CrossRef]
45. Levy, R.C.; Mattoo, S.; Sawyer, V.; Shi, Y.; Colarco, P.R.; Lyapustin, A.I.; Wang, Y.; Remer, L.A. Exploring systematic offsets between aerosol products from the two MODIS sensors. *Atmos. Meas. Tech.* **2018**, *11*, 4073–4092. [CrossRef]
46. Yost, C.R.; Minnis, P.; Sun-Mack, S.; Chen, Y.; Smith, W.L. CERES MODIS Cloud Product Retrievals for Edition 4—Part II: Comparisons to CloudSat and CALIPSO. *IEEE Trans. Geosci. Remote Sens.* **2021**, *59*, 3695–3724. [CrossRef]
47. Minnis, P.; Sun-Mack, S.; Chen, Y.; Chang, F.L.; Yost, C.R.; Smith, W.L.; Heck, P.W.; Arduini, R.F.; Bedka, S.T.; Yi, Y.; et al. CERES MODIS Cloud Product Retrievals for Edition 4—Part I: Algorithm Changes. *IEEE Trans. Geosci. Remote Sens.* **2021**, *59*, 2744–2780. [CrossRef]
48. Kaufman, Y.J.; Tanré, D.; Boucher, O. A satellite view of aerosols in the climate system. *Nature* **2002**, *419*, 215–223. [CrossRef]
49. Quaas, J.; Boucher, O.; Bellouin, N.; Kinne, S. Satellite-based estimate of the direct and indirect aerosol climate forcing. *J. Geophys. Res. Atmos.* **2008**, *113*, 947–955. [CrossRef]
50. An, N.; Wang, K.; Zhou, C.; Pinker, R.T. Observed Variability of Cloud Frequency and Cloud-Base Height within 3600 m above the Surface over the Contiguous United States. *J. Clim.* **2017**, *30*, 3725–3742. [CrossRef]
51. Ma, Q.; Wang, K.C.; He, Y.Y.; Su, L.Y.; Wu, Q.Z.; Liu, H.; Zhang, Y.R. Homogenized century-long surface incident solar radiation over Japan. *Earth Syst. Sci. Data* **2022**, *14*, 463–477. [CrossRef]
52. Wang, K.C.; Dickinson, R.E.; Su, L.; Trenberth, K.E. Contrasting trends of mass and optical properties of aerosols over the Northern Hemisphere from 1992 to 2011. *Atmos. Chem. Phys.* **2012**, *12*, 9387–9398. [CrossRef]